

OVARIAN TRANSCRIPTOMICS OF *D. MELANOGASTER* REVEAL CANDIDATE
GENES UNDERLYING WOLBACHIA-ASSOCIATED
PLASTIC RECOMBINATION

by

SOPHIA I FRANTZ

A THESIS

Presented to the Department of Biology
and the Graduate School of the University of Oregon
in partial fulfillment of the requirements
for the degree of
Master of Science

June 2020

THESIS APPROVAL PAGE

Student: Sophia I Frantz

Title: Ovarian Transcriptomics of *D. melanogaster* Reveal Candidate Genes Underlying Wolbachia-Associated Plastic Recombination

This thesis has been accepted and approved in partial fulfillment of the requirements for the Master of Science degree in the Department of Biology by:

Dr. Nadia Singh	Chairperson
Dr. William Cresko	Chairperson
Dr. Peter Ralph	Member

and

Janet Woodruff-Borden Vice Provost and Dean of the Graduate School

Original approval signatures are on file with the University of Oregon Graduate School.

Degree awarded June 2020

© 2020 Sophia I Frantz

THESIS ABSTRACT

Sophia I Frantz

Master of Science

Department of Biology

June 2020

Title: Ovarian Transcriptomics of *D. melanogaster* Reveal Candidate Genes Underlying Wolbachia-Associated Plastic Recombination

Phenotypic plasticity is prevalent in nature, and its study facilitates understanding of how organisms acclimate to stressful environments. Recombination rate is plastic in a diversity of organisms and under a variety of stressful conditions. However, the recent finding that *Wolbachia pipiensis* induces plastic recombination in *Drosophila melanogaster* deviates from previous patterns, because Wolbachia is not strictly considered a stressor to this host. We investigate the molecular mechanisms of Wolbachia-associated plastic recombination by comparing the ovarian transcriptomes of *D. melanogaster* infected and uninfected with Wolbachia. Our data suggest infection explains a small amount of transcriptional variation but specifically affects genes related to cell cycle, translation, and metabolism. We also find enrichment of cell division and recombination processes. Broadly, the transcriptomic changes identified in this study provide insight for the mechanisms of microbe-mediated plastic recombination, an important but poorly understood facet of host-microbe dynamics.

This thesis includes previously unpublished, co-authored material.

CURRICULUM VITAE

NAME OF AUTHOR: SOPHIA I FRANTZ

GRADUATE AND UNDERGRADUATE SCHOOLS ATTENDED:

University of Oregon, Eugene OR
Swarthmore College, Swarthmore PA

PROFESSIONAL EXPERIENCE:

Graduate Teaching Assistant, Department of Biology, University of Oregon,
Eugene, OR, 2018-2020

Research Assistant, Institute for Genomic Medicine, Columbia University
Medical Center, New York, NY, 2017-2018

Research Assistant, Lewis Sigler Institute for Integrative Genomics, Princeton
University, Princeton, NJ, 2016-2017

TABLE OF CONTENTS

Chapter	Page
I. INTRODUCTION.....	1
II. OVARIAN TRANSCRIPTOMICS OF <i>D. MELANOGASTER</i> REVEAL CANDIDATE GENES UNDERLYING WOLBACHIA-ASSOCIATED PLASTIC RECOMBINATION	2
Introduction	2
Methods.....	6
Results.....	11
1 Wolbachia's Influence on Global Transcription Differences is Variable while the Influence of Genotype is Consistent across Samples.....	11
2 Wolbachia Infection Induces Differential Gene Expression	14
3 Differentially Expressed Genes are Randomly Distributed across the Genome	15
4 Differentially Expressed Genes are Enriched in Cell Division Processes ...	16
Discussion	17
III. CONCLUSIONS	26
APPENDICES	
A. SUPPLEMENTARY FIGURES	27
B. SUPPLEMENTARY TABLES	28
REFERENCES CITED	55

LIST OF FIGURES

Figure	Page
1. Global ovarian transcriptome nMDS ordination.....	11
2. Location of differentially expressed genes across the genome for each chromosome	16

LIST OF TABLES

Table	Page
1. Summary of perMANOVA test results	12

CHAPTER I

INTRODUCTION

Phenotypic plasticity, the phenomenon by which one genotype produces multiple phenotypes in response to different environmental conditions, contributes to phenotypic diversity and is pervasive across a wide variety of taxa (Bradshaw, 1965). Cases of phenotypic plasticity often involve morphological, behavioral or life history traits, but genetic recombination itself can also be plastic (Plough, 1917; Hussin et al., 2011; Stapley et al., 2017). Such plastic recombination has consequences for the genetic diversity of the next generation of a population. Although previous studies have documented many instances of stress-induced plastic recombination, the recent finding that the endosymbiont *Wolbachia pipiensis* induces plastic recombination in its *Drosophila melanogaster* host deviates from these studies (Singh, 2019), since this microbe is not considered a stressor to *D. melanogaster* (Hoffman et al., 1998). Thus, the phenomenon of Wolbachia-induced plastic recombination lies at the intersection of fundamental questions of evolutionary biology, such as the role of phenotypic plasticity in evolution, the determinants of recombination rate variation, and the evolution of host-microbe symbioses. However, an understanding of this phenomenon and its implications for evolution requires an understanding of the molecular basis of Wolbachia-associated plastic recombination. In chapter II, I describe a co-authored study that serves as the initial step toward elucidating the molecular mechanism of Wolbachia-associated plastic recombination. Since recombination occurs in the ovaries and Wolbachia colonize the ovaries, we compared the ovarian transcriptomes of Wolbachia-infected and uninfected flies. We characterized the global ovarian transcriptome response and identify specific

genes that may mediate the interaction between Wolbachia and host recombination processes. I also discuss the implications of this study for understanding plastic recombination and host-microbe interactions.

CHAPTER II

OVARIAN TRANSCRIPTOMICS OF *D. MELANOGASTER* REVEAL CANDIDATE GENES UNDERLYING WOLBACHIA-ASSOCIATED PLASTIC RECOMBINATION

This chapter includes co-authored material. Dr. Nadia Singh designed the experiment and advised with analyses and manuscript preparation. Dr. William Cresko and Dr. Clayton Small advised with analyses and manuscript preparation. I performed all analyses and wrote the manuscript.

Introduction

Under a changing or stressful environment, populations may adapt over generations, and, more immediately, individuals in these populations may acclimate within a lifetime via phenotypic plasticity. Phenotypic plasticity is the phenomenon by which one genotype produces multiple phenotypes in response to different environmental conditions (Bradshaw, 1965). Phenotypic plasticity is pervasive in nature and includes well-studied examples such as seasonal color changes of *Precis octavia* butterflies (Brakefield, 2008) and predator-induced morphological changes in *Daphnia* (Brehm, 1909; Tollrian, 1995). Triggering conditions may be exogenous—such as temperature (Scheepens et al., 2018), or endogenous—such as microbial presence (Verbon & Liberman, 2016).

Although many cases of phenotypic plasticity have involved morphological, behavioral or life history traits, genetic recombination itself can also be plastic (for review see (Modliszewski & Copenhaver, 2017; Stapley et al., 2017). Plastic recombination has been documented in diverse organisms and under a variety of environmental conditions, such as in yeast under osmotic stress (Gao et al., 2008), in

mice under social stress (Balyaev DK & Borodin PM, 1982), and in humans with increasing maternal age (Hussin et al., 2011). The mechanistic link between environmental stress and plastic recombination is largely unknown, though studies in yeast have identified known stress response genes that also regulate recombination rate at specific genomic locations (Gao et al., 2008; Kon et al., 1998). Plastic recombination is a major contributor to variation in recombination rate (Agrawal 2005), and its contribution to genetic diversity overall requires understanding of the conditions in which it manifests.

The study of recombination in the genetic model organism *Drosophila melanogaster* led to key insights about conditions that trigger plastic recombination: recombination was altered in response to extreme temperature (Plough, 1917; Graubard 1932; Grell 1978), starvation (Neel, 1941), and age (Stern, 1926; Hayman and Parsons 1960). Recent work also supports the effect of age (Hunter et al. 2016) and temperature on plastic recombination (Kohl & Singh 2018; Jackson et al. 2015), in addition to other environmental cues such as desiccation (Aggarwal et al. 2019) and parasitic infection (Andronic, 2012; Singh et al. 2015; Zilio et al., 2018). The recent finding that the wMel strain of the endosymbiont *Wolbachia pipiensis* also induces plastic recombination in *Drosophila melanogaster* (Singh, 2019) was surprising in the context of these previous studies of plastic recombination, since wMel is not generally considered a parasite or stressor. Strains of *D. melanogaster* naturally infected with the *wMel* strain of Wolbachia produced a higher proportion of recombinant offspring than individuals of the same strains cleared of *wMel*. Furthermore, of two loci studied, recombination increased at an X-chromosome locus but not at a third chromosome locus, which suggests that

Wolbachia affects recombination at specific regions but perhaps not recombination rate at the genomic scale (Singh 2019).

Although never previously associated with plastic recombination, Wolbachia is a well-studied endosymbiont that resides in the ovaries of its host and is maternally transmitted. It is estimated that up to 40-60% of arthropod species are infected with a species of the Wolbachia genus (Hilgenboecker et al., 2008; Zug & Hammerstein, 2012). The proportion of infected individuals varies by population, with some populations exhibiting very high frequencies of infection (Kriesner et al., 2013; Weeks et al., 2007).

Wolbachia species exert a wide range of effects on their various hosts. In some host species, Wolbachia infection is classified as harmful, causing reduced reproductive output through four main mechanisms: cytoplasmic incompatibility (CI), male-killing, feminization, and parthenogenesis (for review see Werren et al., 2008). These mechanisms often ensure Wolbachia's propagation to the next generation. Theoretical and empirical evidence also suggests these parasitic interactions can evolve to become more mutualistic over time (Ballard, 2004; Weeks et al., 2007). In other species, Wolbachia currently confers advantages such as increased reproductive output and protection from viral infection (Vavre et al., 1999). Some species receive essential nutrients from Wolbachia (Brownlie et al., 2009; Hosokawa et al., 2010), and *Drosophila paulistorum* even presents an extreme example of obligate mutualism in which Wolbachia is needed for gonad development (Miller et al. 2010).

These examples show that the effect of Wolbachia strongly depends on the particular host species and genotype as well as the strain of Wolbachia. In its *D. melanogaster* host, *wMel* induces only weak CI in laboratory strains and even weaker CI

in the wild (Hoffman et al., 1998). Therefore, its high global infection rate of an estimated 34% in wild populations of *D. melanogaster* cannot be explained by reproductive manipulation through CI alone and may instead be explained by benefits conferred to the host (Solignac et al., 1994; Serga et al., 2014). Benefits such as increased survival and fecundity have been documented in *wMel*-infected strains of *D. melanogaster* (Fry & Rand, 2002; Fry et al., 2004). In fact, the same strains that exhibit increased recombination with Wolbachia infection also exhibited increased reproductive output (Singh, 2019).

Despite this evidence that *wMel* is beneficial to its *D. melanogaster* host, it also induces increased recombination, a trait more often associated with stressful conditions. This novel mediator of plastic recombination and its ambiguous relationship to stress prompted us to investigate the molecular mechanisms that mediate Wolbachia-associated plastic recombination. We posited that the molecular mechanism underlying increased recombination in Wolbachia-infected flies would be reflected in host transcriptional changes. We therefore performed RNA-sequencing and differential expression analysis to compare the transcriptomes of Wolbachia-uninfected and infected flies. Since the ovaries are the site of both Wolbachia colonization and meiotic recombination, we sequenced the ovarian transcriptome. We sought to characterize global ovarian transcriptome changes and identify candidate genes that mediate *Wolbachia*-associated plastic recombination. The use of four different strains of *D. melanogaster* allowed us to disentangle transcriptional variation due to infection, genotype, and the interaction of infection and genotype. The latter process has never been addressed in this host-symbiont system. Our data suggest the contribution of Wolbachia to ovarian transcriptional variation is limited,

variable, and mediated by the host genotype. The data also suggest the observed increased recombination cannot be explained by increased genome-wide or locus-specific transcription. Finally, we identified a subset of genes with functions in cell division, translation, and metabolism that are differentially regulated under Wolbachia infection.

Methods

Drosophila stocks

We used four strains from the Drosophila Genome Reference Panel (DRGP) (Mackay et al., 2012) for this study: RAL73, RAL783, RAL306, and RAL853. These lines have standard chromosome arrangements and are naturally infected with *Wolbachia pipiensis* (Huang et al., 2014). Genomic analysis suggests this strain of Wolbachia is closely related to *wMel* (Richardson et al., 2012). To generate Wolbachia-uninfected flies, we raised flies on media containing tetracycline at a concentration of 0.25 mg/mL for two generations. To reintroduce the natural microbiome without Wolbachia, uninfected flies were subsequently raised on standard food for at least ten more generations before transcriptome data were obtained (Singh, 2019). Wolbachia infection status was confirmed prior to experimentation using a PCR-based assay with Wolbachia-specific primers (Jeyaprakash & Hoy 2000). Infection status was also confirmed for each sample after RNA-sequencing by quantifying the number of reads that aligned to the Wolbachia reference genome. Flies were kept at 25 degrees on a 12:12 light:dark cycle.

Ovary dissections and sequencing

We placed anesthetized three-day-old virgin females in phosphate-buffer saline, dissected their ovaries, and froze the ovaries on dry ice. We prepared 4 replicates of each of the 4

genotypes for each infection status, with 10 pairs of pooled ovaries comprising each replicate. Dissections, library preparations, and sequencing were performed in two batches two months apart: all dissections on the RAL783 and RAL73 samples were performed on one day, and all dissections of RAL306 and RAL853 were performed in one day two months later. Each replicate of 10 pairs of ovaries remained frozen until library preparation using Illumina TruSeq RNA prep kit. RNA libraries were prepared and sequenced at the University of Oregon Genomics and Cell Characterization Core Facility. Libraries were sequenced on a HiSeq 4000 using single end, 150-bp reads.

Sequence processing and alignment

Raw reads were aligned to the *Drosophila melanogaster* reference genome from the Berkeley Drosophila Genome Project (BDGP) assembly release 6 with STAR aligner v. 2.5.3a (Dobin et al., 2013) with default parameters. Batch 1 (comprised of strains RAL73 and RAL783) generated an average of 22,443,144 reads with 98% aligning uniquely to the reference genome, and batch 2 (comprised of RAL306 and RAL853) generated on average 21,936,370 reads with 89% aligning uniquely to the reference genome (Supplementary Table 1). Because of this clear difference in sequencing statistics and the fact that samples were prepared and sequenced in two batches, we performed all analyses separately for each batch.

Differential expression analysis

All analyses were conducted in R v. 3.4.3. For each sample we counted the number of uniquely mapped reads using GenomicAlignments v. 3.6-intel-2017b (Lawrence et al., 2013) with default parameters. We then used DESeq2 (Love et al., 2014) to perform differential expression analysis on gene count data. Specifically, we fit a model of

expression level for each gene as determined by the effect of infection status, while controlling for genotype and the interaction of infection status and genotype. DESeq2 uses a model particularly suited for the overdispersion of RNA-seq data based on the negative binomial distribution. We set the uninfected samples as the base level, so “upregulation” refers to higher normalized read counts in the infected flies. DESeq2 uses the Benjamini and Hochberg (1995) method by default to control the false discovery rate (FDR). We define differentially expressed genes as those with a \log_2 fold change greater than 0, after controlling the FDR at 0.05. We chose this threshold of $> 0 \log_2$ fold difference based on the premise that genes in the recombination pathway are precisely regulated so that even a small change in expression levels could reflect a functional change in meiosis (Reynolds et al., 2013; Ziolkowski et al., 2017). We identified differentially expressed genes in batch 1 and batch 2 separately.

Multivariate Analysis with nMDS and perMANOVA

To visualize differences in expression among 17,377 transcripts across all samples, we used Bray-Curtis dissimilarity to generate an nMDS ordination plot. We quantified the percentage of dissimilarity explained by infection status, genotype, and the interaction of infection and genotype with a permutational multivariate analysis of variance (perMANOVA) test. We controlled for batch by performing the test separately on each of the two batches and for genotype by limiting permutations to samples within genotypes. We used the R package vegan v. 2.5-5, (Okasanen et al., 2019) to calculate distances, plot nMDS, and perform the perMANOVA test.

Outlier Ordination

Initial visualization with an nMDS plot revealed that sample RAL73 Wolbachia-infected A (RAL73 w+A) differed from the other three replicates of RAL73 infected samples, as well as all other samples in this study. To determine whether this sample represented an outlier with significant influence on the results of the differential expression analysis, we examined Cook's distance on the normalized count data, as calculated by DESeq2. A higher Cook's distance for a sample indicates more leverage in determining a given transcript's fold change. We compared the average Cook's distance for each sample across all transcripts and the number of times each sample contained the highest Cook's distance for each transcript (Supplementary Figure 1). Replicate samples should not differ much in their distribution of Cook's distances, but we found that the average Cook's distance for sample RAL73w+ replicate A was much higher than all other samples and most often contains the maximum Cook's distance across all transcripts. These results suggest sample RAL73w+A has aberrant expression of many genes. Although DESeq2 can manage outliers for transcripts of genes if there are replicates of each factor, we decided that a sample which consistently contains an outlier across many genes likely represents not true biological signal but rather an error of preparation. This distribution of Cook's distances led us to exclude RAL73w+A from all subsequent analyses.

Gene Ontology Analysis

We identified Gene Ontology (GO) descriptions for the differentially expressed genes using the Panther biological process classification system, as implemented in Panther's data mapping online tool (Thomas et al, 2003). Panther classifies each GO term into nested levels, and we report the level of nesting for GO terms in order to provide more

specific information. We then tested whether any GO terms were overrepresented in each group of differentially expressed genes using Panther's statistical overrepresentation test, which uses Fisher's exact test (Fisher, 1954) with False Discovery Rate (FDR) controlled at 0.1 and all annotated genes in the *Drosophila melanogaster* genome as reference.

Distribution of DE Genes Across Genome

To test whether differentially expressed genes are randomly distributed across the genome, we performed a non-parametric run's test for randomness (Bradley, 1968). We categorized each gene as differentially expressed or not, based on the same criteria of \log_2 fold change > 0 and FDR controlled at 0.05. We then placed each gene's differential expression information in order of placement across the genome, using the gene start site as the location. A switch from differentially expressed to not, or vice-versa, was considered a complete run. We visualized these patterns of gene expression across the genome with the R package karyoplotR (version 1.8.8; Gel & Serra 2017). For each chromosome, we depict the differentially expressed genes at their location in the BDGP6 *D. melanogaster* reference genome.

Results

Wolbachia's influence on global transcriptional differences is variable while the influence of genotype is consistent across samples

To understand the relative extent to which transcriptional variation depends on Wolbachia infection status and genotype, we visualized this variation across samples with an nMDS plot (Figure 1a). The strongest biological pattern in this plot is the grouping of samples based on genotype. Samples of the same genotype are often associated with each

other regardless of infection status. The plot also recapitulates the batch effect, since the cluster of samples prepared in the first batch (RAL73 and RAL783) is distinct from the cluster of samples prepared in the second batch (RAL306 and RAL856). Plotting samples from each batch on a separate nMDS plot suggests both genotype and infection status contribute to transcriptional differences among samples in batch 1 (Figure 1b). In contrast, the nMDS plot for the batch 2 samples alone (Figure 1c) suggests that genotype is a strong determinant of transcriptional differences while infection status is not. Overall, these plots suggest the contribution of *Wolbachia* to global ovarian transcriptional variation is subtle but depends on genotype, while genotype consistently accounts for transcriptional differences in these samples.

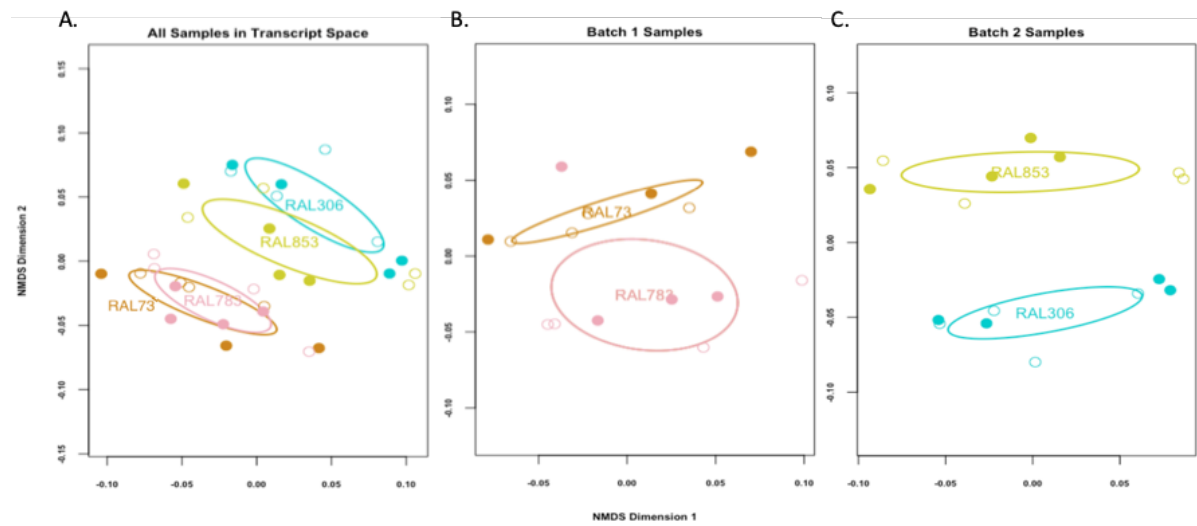


Figure 1. Global ovarian transcriptome nMDS plots. Each sample is represented in 2-dimensional transcript space with a circle, with open circles representing uninfected samples and filled circles representing infected samples. Each genotype is depicted with a different color. The ellipses mark the 95% confidence intervals of the centroid for the samples from each genotype. **a)** The samples cluster based on genotype and infection status, with genotype contributing to the most obvious clustering. The batch effect is also visible: the RAL73 and 783 samples form a cluster while the RAL306 and RAL853 samples form a separate cluster. **b)** Dissimilarity was calculated only between samples in batch 1. Samples cluster by genotype and infection status. **c)** Dissimilarity was calculated only between samples in batch 2. The samples group by genotype and there is no obvious grouping by infection status.

To quantify the patterns observed in the nMDS plot, we used a permutational multivariate analysis of variance (perMANOVA) test to estimate the percent of variation in gene expression explained by infection status, genotype, and the interaction of these factors (Table 1). Consistent with the nMDS patterns, the perMANOVA results suggest that genotype accounts for a large and statistically significant proportion of variation in both batch 1 ($R^2 = 0.17, P = 0.006$) and batch 2 samples ($R^2 = 0.26, P = 0.01$). For batch 1, infection status explains a similarly large percent of variation as does genotype ($R^2 = 0.19, P = 0.003$). In batch 1, the interaction of genotype and infection also had a notable effect that was statistically significant ($R^2 = 0.13, P = 0.02$). This interaction means Wolbachia's contribution to transcriptional differences in these samples depends on host genotype (for RAL73 or RAL783).

In contrast, infection status accounts for a smaller and non-significant proportion of transcriptional variation among samples in batch 2 ($R^2 = 0.06, P = 0.3$). Consistent with the small effect of infection status, the interaction effect for the samples in batch 2 was also small and nonsignificant ($R^2 = 0.06, P = 0.28$). In conclusion, genotype and infection status contribute about equally to the variation in transcription among the samples in batch 1, whereas genotype accounts for much more of the variation than does infection status in batch 2. The contribution of infection status to host gene expression varies, while the contribution of genotype is consistently large and significant in these samples.

factor	batch 1					batch2				
	df	meanSS	F-value	R2	p-value	df	meanSS	F-value	R2	p-value
infection	1	0.007	4.08	0.19	0.003	1	0.003	1.103	0.057	0.3
genotype	1	0.006	3.66	0.17	0.006	1	0.015	5.018	0.259	0.01
infection:genotype	1	0.005	2.73	0.127	0.024	1	0.004	1.222	0.063	0.28
Residuals	11	0.002		0.51		12	0.003		0.62	

df - degrees of freedom, meanSS - mean sum of squares. p-values are based on 1000 permutations

Table 1. Summary of perMANOVA test results. Infection status and genotype explains a large and significant proportion of the dissimilarity among samples in batch 1 while genotype alone explains the largest proportion of accounted dissimilarity in batch 2. The perMANOVA is based on Bray-Curtis dissimilarities using gene expression differences across samples. The test was performed separately for each batch.

Wolbachia infection induces differential gene expression in D. melanogaster

The transcriptional profile of Wolbachia infection can also be described by the individual genes that are differentially regulated in Wolbachia-infected flies as compared to uninfected flies. In batch 1, 1104 genes (6% of all transcripts) are differentially expressed, with 618 upregulated in *Wolbachia*-infected flies and 486 downregulated. The differentially expressed genes, along with their fold change, direction of change, mean number of counts, test statistic, and adjusted p-values sorted in ascending order are shown in Supplementary Table 1. In batch 2, 96 genes (0.5% of all transcripts) are differentially expressed, with 36 upregulated and 60 downregulated genes (Supplementary Table 2). This difference between the number of genes identified in the two batches is consistent with the finding that infection status does not account for a large proportion of global transcriptional differences in batch 2. We compared the sets of genes from the two batches to identify the genes consistently differentially expressed across these samples despite genotype and batch differences. There are 26 genes in common between batches, shown in Supplementary Table 3.

Differentially expressed genes are randomly distributed across the genome

In the Drosophila early ovarian transcriptome, genomic regions with higher rates of transcription also have higher rates of recombination (Adrian and Comeron 2013). Since Wolbachia infection leads to increased recombination at certain genomic regions (Singh 2019), we tested whether infection may also be associated with altered levels of transcription at certain genomic regions. To do so, we performed runs test for randomness (Bradley 1968) to determine whether a binary sequence of items (differentially expressed or not) is random. We performed the runs test for each chromosome arm and did not reject the null hypothesis of randomness each time, which suggests the location of differentially expressed genes across the genome is random. This random placement of DE genes across each chromosome arm is illustrated in Figure 2. The visualization and runs test results provide no evidence that Wolbachia infection is associated with differential expression of genes at particular genomic locations.

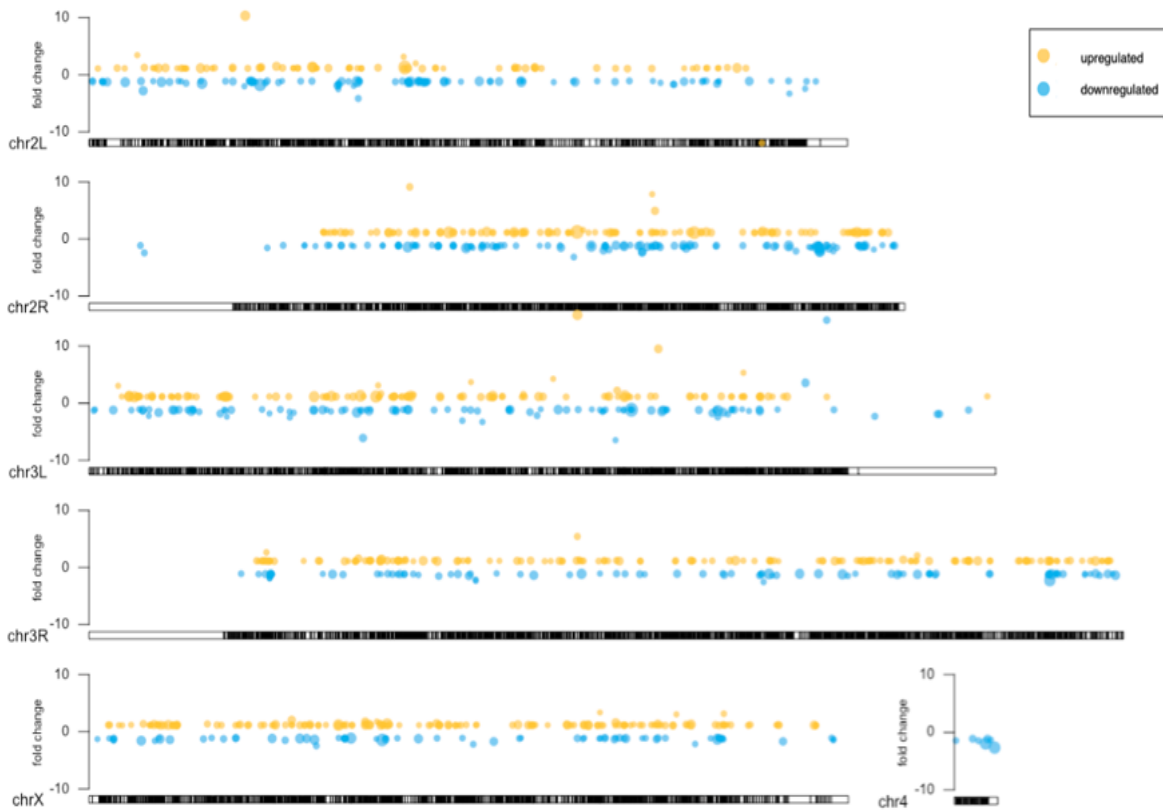


Figure 2. Location of differentially expressed genes from batch 1 across the genome for each chromosome. Differentially expressed genes are distributed randomly across the genome as determined by the runs test for randomness. Genes with $> 0 \log_2$ fold change expression difference and with an adjusted p-value < 0.05 are shown at their position on the chromosome, represented by the ideogram. Each circle represents a gene. The placement of the circle on the fold change axis shows the value of fold change difference when comparing uninfected and infected samples. The size of the circle is proportional to the range of p-values for all DE genes, with the biggest circles corresponding to the smallest p-values. Yellow represents upregulation and blue represents downregulation.

Differentially expressed genes are enriched in cell division processes

To better understand the function of these differentially expressed genes, we associated each gene with its most nested biological process GO terms (Thomas et al. 2003, Huaiyu et al. 2010) and tested for overrepresentation of these terms. In batch 1, the 1104 differentially expressed genes contained significant overrepresentation of 99 GO terms. These GO terms are provided in Supplementary Table 5, sorted in order of highest to lowest enrichment score. The three most overrepresented terms are “spindle midzone

assembly” (enrichment = 12.89, FDR = 0.008), “cytoplasmic translation” (enrichment = 8.56, FDR = 0.0001), and “mitotic spindle elongation” (enrichment = 8.06, FDR = 0.027). Among the enriched terms were other cell cycle-related processes such as “centrosome separation” (enrichment = 6.78, FDR = 0.001) and “meiotic cytokinesis” (enrichment = 3.15, FDR = 0.033). Other common terms were those related to translation, such as “ribosomal small subunit assembly” (enrichment = 6.45, FDR = 0.001). Since batch 2 has only 96 differentially expressed genes, the statistical power to determine overrepresentation of GO terms was limited. With a FDR threshold of 0.1, no GO terms were significantly enriched. To get a sense of the genes’ processes we looked at the 55 GO terms with a raw *P*-value below 0.05 (Supplementary Table 6). The top terms in batch 2 are “N-acetylneuraminate catabolic process,”, “regulation of histone H4 acetylation involved in response to DNA damage stimulus,”, and “maintenance of rDNA” (enrichment > 100, *P* = 0.013 for all three terms). GO terms related to cell division processes are not among the most enriched in this small set of genes, but relevant terms include “synaptonemal complex assembly” (enrichment = 26.07, *P* = 0.04) and “female meiosis sister chromatid cohesion” (enrichment = 78.22, *P* = 0.019).

Discussion

Global transcription patterns suggest a consistent effect of genotype and variable influence of Wolbachia infection

Other experiments from a wide range of model systems support our finding that genotype significantly contributes to differences in global transcription (Hutter et al., 2008; Poelstra et al., 2014) and is consistent with evidence that variation in gene

expression is heritable (Brem et al., 2002; Dixon et al., 2007). In fact, these same *D. melanogaster* strains (DGRP) were used to quantify transcriptional differences due to genotype (Huang et al., 2015). Of 18,140 genes measured in the Huang et al. study, 42% showed significant variability in expression levels due to genotype. In our study, 11% of genes are differentially expressed when comparing RAL73 to RAL 783, and 16% of genes are differentially expressed when comparing RAL306 to RAL853 (while controlling for infection status). The larger percentage found in the Huang et al. study may be attributed to their quantification of variation across 205 strains versus across two strains (per batch) in our study.

In contrast to the consistent effect of genotype, we found that the differences in transcription explained by Wolbachia infection were variable between the two batches. Wolbachia infection explained a small and non-significant proportion of variation in batch 2, but it explained approximately as much variation as genotype in batch 1. These differences in the explanatory power of infection could be due to greater transcriptional differences between samples within RAL306 and RAL853 that limit the power to detect variation due to infection status. The results could also reflect true biological differences in the degree to which *Wolbachia* affect ovarian transcription in different genotypes. A combination of explanations could be true, and future studies will be needed to disentangle the transcriptional variation due to technical versus biological differences between batches.

Though we cannot parse out the differences due to genotype versus batch across all four genotypes studied, we can compare the effect of genotype within each batch. We found a significant interaction between genotype and infection status for the samples in

batch 1, suggesting the effect of Wolbachia on transcription depends on the genotype of the host. This result has never been documented for *Wolbachia*'s effect on the ovarian transcriptome. However, that a microbe's effect depends on host genotype is increasingly documented in many systems (Ko et al., 2009; Mateus et al., 2019; Small et al 2017). The phenotypes associated with Wolbachia vary widely by host, ranging from neutral to parasitic to mutualistic. Our finding shows that the specificity of Wolbachia's relationship to its host also applies to different genotypes within the same species and that this specificity is reflected at the transcriptional level.

*Global transcription patterns reflect symbiosis between *D. melanogaster* and *W. pipiens**

We found that Wolbachia infection did not explain the majority of transcriptional variation among these samples. Although certain microbial infections significantly alter host transcription of many genes (Aprianto et al., 2018; Camilios-Neto et al., 2014; Rienksma et al., 2019), other infections exert a more limited effect (Rawls et al. 2004; Camp et al. 2014; Small et al., 2017). Parasitic and obligately mutualistic microbes often impose sweeping changes to host transcription. For example, a study of host tissue-specific transcriptional response to the pathogenic bacterium *Yersina pseudotuberculosis* revealed substantial changes in expression. 1,336 genes had at least a four-fold change in expression (Nuss et al., 2017), while our study identified only 210 and 154 genes with this extreme fold change in batch 1 and batch 2. Manipulations of obligately mutual microbes have also revealed sweeping changes to the host transcriptome (Bing et al., 2017; Mateus et al., 2019). While Wolbachia is considered an obligate mutualist in some hosts (Miller et al. 2010; Taylor et al. 2010) and exerts parasitic effects in other hosts (Bourtzis et al., 1996), it does not exhibit this extreme

relationship with *D. melanogaster*, and the limited and variable transcriptional changes we observe is consistent with this form of symbiotic relationship

Genomic Location of DE genes does not support model of increased recombination via increased transcription

We found that genes with differential expression in *Wolbachia*-infected flies were randomly distributed across each chromosome arm. We also found that the differentially expressed genes had approximately equal levels of upregulation and downregulation. These findings are in contrast to a model in which recombination increases with *Wolbachia* infection because *Wolbachia* cause upregulation of genes. We tested this hypothesis because across many eukaryotes, sites of recombination are correlated with sites of increased transcription (Aguilera & Gaillard, 2014), and it is proposed that this correlation arises because transcription promotes recombination to resolve genomic instability (Gottipati & Helleday, 2009). This correlation exists in *D. melanogaster*, as genes with ovarian transcription above 1 FPKM are concentrated in sites of known recombination (Adrian & Comeron, 2013). If the observed increase in recombination at the X-chromosome locus associated with *Wolbachia* infection (Singh, 2019) was due to increased transcription in this region, then we would observe higher numbers of upregulated genes at this region. We instead observe approximately equal numbers of upregulated and downregulated genes at this region. We looked at this region in particular because we know it is associated with increased recombination under *Wolbachia* infection, but it is also possible that *Wolbachia* could increase transcription at other genomic locations we have not yet quantified. However, this trend of randomness extends to the rest of the genome: upregulated genes are distributed evenly across the

genome, and we see approximately equal distribution of upregulated and downregulated genes (Figure 2). The equal distribution of differentially expressed genes across the genome and the similarity in the numbers of up- and down-regulated genes does not support the hypothesis that *Wolbachia* infection promotes increased recombination via increased transcription.

Differentially expressed genes overlap with previous meiosis studies

We found 1,104 genes differentially regulated with *Wolbachia* infection in batch 1, and 96 genes in batch 2. We were interested in characterizing changes in gene transcription to identify candidate genes that mediate *Wolbachia*-associated plastic recombination. Previous research supports a connection between altered gene expression and altered recombination, as some recombination genes are known to affect recombination in a dosage-sensitive manner (Reynolds et al., 2013; Ziolkowski et al., 2017). Although genes underlying other *Wolbachia*-induced phenotypes such as cytoplasmic incompatibility have been identified (Beckmann et al., 2017; LePage et al., 2017), the genetic basis of *Wolbachia*-associated plastic recombination is unknown. Since the X-chromosome interval was previously found to exhibit increased recombination in *Wolbachia*-infected flies (Singh, 2019), we compared our differentially expressed genes to a list of 111 genes significantly associated with variation in recombination at the X-chromosome locus as determined by a GWAS (Hunter et al., 2016). We found ten genes in common between these two studies: *Pka-C3*, *px*, *ND-23*, *oat*, *DAAM*, *Tgi*, *dpr6*, *spri*, *Msp3000* (batch 1), and *CG11200* (batch 2). These genes do not have annotated functions in meiosis, suggesting an unknown mechanism for modifying recombination rate. In addition to commonalities with this association study,

we also found commonalities with a list of 25 genes from a 2002 review paper of experimentally-confirmed meiosis genes (McKim et al., 2002). Four genes reviewed in this paper were differentially expressed in our study: *c(2)m*, *sub*, *ncd* (batch 1), and *ord* (batch 2). Among the genes involved in early meiosis is *c(2)m*, which is involved in SC assembly. Since *c(2)m* suppresses crossovers (Manheim & McKim, 2003), its significant downregulation in batch 1 may act to release the suppression of crossovers, ultimately resulting in more crossovers during meiosis. We also identified genes known to be involved in late meiosis, *sub* and *ncd*, which both play a role in the formation of the meiotic spindle pole. This combination of early and late meiosis genes provides an avenue of further study into the mechanisms of Wolbachia-induced plastic recombination.

GO terms provide direction for future experiments investigating cell cycle processes

The percent of the transcriptome affected in our study (6% and 0.5%) is similar to a previous study which also did not find large-scale changes in transcription. He et al. (2019) found that 296 genes (2.2%) were differentially expressed when comparing ovaries of *D. melanogaster* infected and uninfected with Wolbachia. Also consistent with this limited effect, a study of the *D. melanogaster* and *D. simulans* ovarian proteome found 61/549 proteins (11%) were differentially regulated in *D. melanogaster* and 49/449 (11%) were differentially regulated in *D. simulans*. Though these two studies and ours are the only ones that specifically focus on the ovarian activity of *D. melanogaster* under Wolbachia infection, a number of others have characterized the transcriptomic response to Wolbachia infection in various species and tissues. These studies confirm the effect of Wolbachia depends on the host, as different processes were found to be affected,

including reproduction, immunity, and stress response (Brennan et al., 2008; Chevalier et al., 2012; Hughes et al., 2011; Kremer et al., 2012; Pan et al., 2012; Rao et al., 2012; Xi et al., 2008; Zheng et al., 2011).

The differentially expressed genes from batch 1 are enriched in processes related to mitotic and meiotic cell division. Five of the top six most enriched significant GO terms are related to late cell division processes including chromosome segregation: “spindle midzone assembly”, “mitotic spindle elongation”, “kinetochore organization”, “attachment of spindle microtubules to kinetochore”, and “mitotic spindle assembly checkpoint”. Some genes in batch 2 are also associated with cell division functions, suggesting that altered cell division is consistently associated with Wolbachia infection in these samples. Our finding that genes associated with cell division processes are differentially regulated in Wolbachia-infected flies is consistent with the study by Christenson et al. 2016, which found that a cell division suppressor protein 14-3-3 zeta was downregulated in Wolbachia-infected flies. Furthermore, the transcriptomic changes to cell division is consistent with a previously documented phenotype associated with Wolbachia—increased mitosis in germline stem cells associated with a four-fold increase in egg production in *D. mauritiana* (Fast et al., 2011). Previous work on two strains used in this study, RAL306 and RAL853, also suggest that Wolbachia infection is associated with increased reproductive output (Singh, 2019). Together, these findings merit further investigation into how Wolbachia influence both increased reproductive output and increased proportion of recombinant offspring.

In contrast to our study, the He et al. 2019 study did not identify any GO terms related to cell division functions. The differences in results could be related to the

different genotypes used for the different studies. Although our study included multiple genotypes, it did not include the genotype studied previously (He et al. 2019). Given that genotype has a large effect on transcription in *D. melanogaster* and that our data indicate transcriptional variation due to infection depends on host genotype, the differences between the two studies may result from differences in genotypes employed in the experiments, and future studies should address this variation by including a diversity of genetic backgrounds.

Other enriched terms are consistent with previous studies of the effect of Wolbachia infection on host transcription

We found a number of other processes enriched in Wolbachia-infected flies that can largely be grouped into two categories: metabolism and translation. The finding that metabolism is affected by Wolbachia infection is not surprising since altered metabolism is frequently associated with host-microbe interactions (Maslowski, 2019). Wolbachia infection is associated with depletion of certain classes of lipids in the mosquito *Aedes albopictus* (Molloy et al., 2016), increased host resistance to iron depletion (Brownlie et al., 2009), and altered host production of dopamine-dependent arylalkylamine N-acetyltransferase (Grunenko et al., 2017). We also found altered N-acetylneuraminate catabolism associated with Wolbachia infection in our study, along with other metabolic processes such as “negative regulation of insulin secretion,” “glucosamine catabolic process,” “glutathione metabolic process,” and “chitin metabolic process.” Altered metabolism was found in the two other studies of Wolbachia-infected ovaries of *D. melanogaster*: Christenson et al. (2016) found differential levels of proteins related to

carbohydrate transfer and metabolism, and He et al. (2019) find differential regulation of starch and sucrose metabolism genes.

Apart from altered cell division, we found the processes most affected by Wolbachia infection are those related to translation, protein synthesis, and ribosome synthesis. Furthermore, most of these differentially expressed genes are downregulated. These results are consistent with Christenson et al 2016, who also found downregulation of protein synthesis proteins in both Wolbachia-infected *D. melanogaster* and *D. simulans*. Interestingly, a recent study found that perturbing assembly of translation components through RNAi results in increased Wolbachia titer, further supporting a link between decreased translation and Wolbachia infection (Grobler et al., 2018).

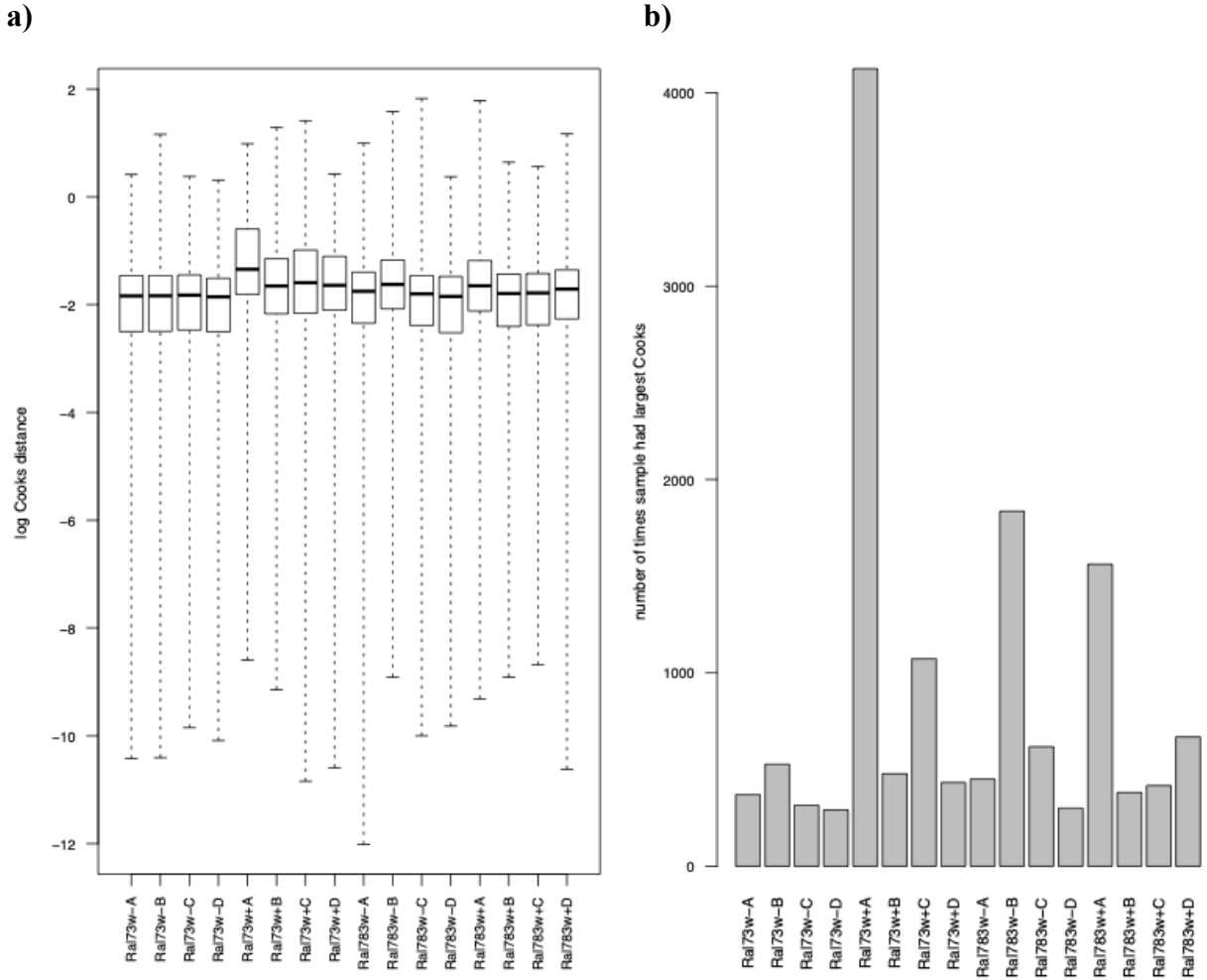
CHAPTER III

CONCLUSIONS

We investigated how ovarian transcription is altered with Wolbachia infection in this interesting host-microbe system, particularly with respect to increased recombination in the host. We found that Wolbachia infection contributes in a limited and variable way to host ovarian transcription. We demonstrate for the first time that Wolbachia's effect on ovarian transcription is mediated by the host's genotype. We found that altered ovarian cell division processes are associated with Wolbachia infection and identified a set of candidate genes that will allow us to further explore the link between Wolbachia infection and increased recombination. The downregulation of *c(2)m* in Wolbachia-infected flies, along with its known role as a suppressor of crossovers (Manheim & McKim, 2003), make this gene a promising candidate for future studies. For example, we would like to specifically quantify its expression with more precise methods such as qPCR or microscopy of the synaptonemal complex. We would also like to test its role in plastic recombination, perhaps by testing whether down-regulation of *c(2)m* in Wolbachia-uninfected flies recapitulates the recombination phenotype of Wolbachia infection. Other genes of interest include the genes involved in spindle and kinetochore processes (e.g. *sub*, *polo*, *incenp*), which are highly enriched terms in Wolbachia-infected flies. These identified transcriptomic changes will guide future studies of Wolbachia's symbiosis with its *D. melanogaster* host and its relation to plastic recombination.

APPENDIX A

SUPPLEMENTARY FIGURES



Supplementary Figure 1: Outlier investigation through metrics of Cook's distance. **a)** For every transcript with count data, Cook's distance was measured for each sample. The distribution of log Cook's distances for each sample is shown. RAL73w+ has higher average Cook's distance than the rest of the samples. **b)** The number of times each sample had the highest Cook's distance for a given transcript is plotted. RAL73w+A most often has the highest Cook's distance.

APPENDIX B
SUPPLEMENTARY TABLES

Batch 1			Batch 2		
sample ID	# reads mapped	% reads mapped	sample ID	# reads mapped	% reads mapped
RAL73w - A	25,580,060	98.21	RAL306w - A	30,181,092	89.9
RAL73w - B	23,340,083	97.67	RAL306w - B	21,532,464	88.6
RAL73w - C	23,830,990	98.1	RAL306w - C	29,151,147	89.87
RAL73w - D	23,886,917	98.18	RAL306w - D	24,077,440	86.97
RAL73w + A	23,461,064	98.14	RAL306w + A	25,333,773	90.52
RAL73w + B	22,213,114	98.15	RAL306w + B	23,015,730	90.09
RAL73w + C	22,414,516	98.25	RAL306w + C	21,057,850	90.57
RAL73w + D	20,165,444	98.2	RAL306w + D	19,633,517	90.35
RAL783w - A	24,508,882	98.29	RAL853w - A	20,800,548	90.93
RAL783w - B	21,975,849	97.75	RAL853w - B	16,410,190	90.76
RAL783w - C	20,906,567	98.09	RAL853w - C	22,790,031	87.11
RAL783w - D	22,989,934	98.2	RAL853w - D	18,623,251	89.76
RAL783w + A	20,287,678	98.22	RAL853w + A	23,365,471	90.6
RAL783w + B	21,266,231	98.04	RAL853w + B	15,723,826	89.15
RAL783w + C	21,347,772	98.01	RAL853w + C	22,380,358	88.8
RAL783w + D	20,915,208	97.94	RAL853w + D	16,905,243	90.06
mean 22,443,144		mean 98.09	mean 21,936,370		mean 89.63

Supplementary Table 1: Sequencing Statistics. Shown are the sample ID for batch 1 and batch 2, the total number of reads that mapped uniquely to the genome for each sample, and the percent of total reads that mapped uniquely to the genome. The mean number and percentage across samples in each batch are also shown.

Supplementary Table 2. Differentially expressed genes identified in batch 1. Base mean is the number of transcripts averaged across all samples. “Direction” indicates whether the gene is up- or downregulated. Genes are listed in order of ascending p-values.

FlyBase ID	geneSymbol	basemean	direction	foldchange	adjpvalue
FBgn0015371	:chn	5824.695351	+	1.242944392	4.83E-07
FBgn0021768	:nudC	2340.511398	-	0.869184226	4.83E-07
FBgn0032147	:IP3K1	789.6364932	+	1.289066087	6.10E-07
FBgn0259682	:Jabba	21855.91971	+	1.102041432	3.33E-06
FBgn0016076	:vri	261.3155352	-	0.565178485	4.97E-06
FBgn0052708	:CG32708	431.3725013	-	0.692267163	5.57E-06
FBgn0020633	:Mcm7	4617.717077	+	1.154391425	1.08E-05
FBgn0053653	:Cadps	270.590133	-	0.377188227	1.13E-05
FBgn0039932	:fuss	159.6121195	-	0.514481512	1.36E-05
FBgn0262112	:sro	84.25678352	-	0.443607451	1.38E-05
FBgn0033581	:CG12391	3975.734575	+	1.159713313	1.94E-05
FBgn0036646	:CR18217	1690.904761	+	1.225095393	1.94E-05
FBgn0265102	:Oseg1	1004.471516	+	1.29812973	2.47E-05
FBgn0260866	:dnr1	292.2428768	-	0.701333426	2.73E-05
FBgn0029957	:CG12155	1176.091848	+	1.153835107	3.26E-05
FBgn0032015	:Ostgamma	1340.420367	-	0.838754136	6.20E-05
FBgn0024754	:Flo1	666.0053172	-	0.787070186	6.49E-05
FBgn0030000	:CG2260	1236.423903	-	0.88499688	6.49E-05
FBgn0260768	:CG42566	245.2622479	-	0.465663749	6.57E-05
FBgn0052533	:CG32533	499.7868225	-	0.761070149	7.08E-05
FBgn0014396	:tim	660.8207665	-	0.660169486	7.17E-05
FBgn0267487	:Ptp61F	6957.069963	+	1.105612863	7.17E-05
FBgn0001104	:Galphi	5342.231339	+	1.144087569	7.84E-05
FBgn0260789	:mxc	4133.962333	+	1.372242076	7.84E-05
FBgn0003257	:r-I	2584.838299	-	0.869777302	0.000115165
FBgn0032518	:Rpl24	27914.02068	-	0.822636133	0.000115165
FBgn0062928	:hpRNA:CR33940	1639.123453	-	0.790326747	0.000115165
FBgn0033459	:CG12744	749.0956185	-	0.70494348	0.000116233
FBgn0004378	:Klp61F	3094.420953	+	1.186528335	0.000126446
FBgn0026404	:Dronc	2155.559866	+	1.240488336	0.000126446
FBgn0034908	:CG5543	761.0781579	+	1.181190052	0.000126446
FBgn0002466	:sti	3074.874497	+	1.230995302	0.000129151
FBgn0034654	:elf3k	5468.215446	-	0.814063198	0.000129151
FBgn0040491	:Buffy	97.40692998	-	0.63692215	0.000129151
FBgn0034761	:CG4250	307.4417229	-	0.601876385	0.000140453
FBgn0035868	:CG7194	159.9505488	-	0.6229709	0.000149962
FBgn0031868	:Rat1	1836.721068	+	1.36620718	0.000167712
FBgn0035793	:CG7546	4476.285204	+	1.22880714	0.000172474
FBgn0053138	:AGBE	3073.312161	+	1.170254307	0.000180354
FBgn0261284	:bou	175.0946579	-	0.714588537	0.000215164
FBgn0267160	:asRNA:CR45600	22.23387348	+	44.20150074	0.000215164
FBgn0052281	:CG32281	365.8190556	-	0.76059762	0.000217978
FBgn0011692	:pav	3121.18654	+	1.157805166	0.000226133
FBgn0016691	:ATPsynO	4441.612507	-	0.887885127	0.000226133
FBgn0002622	:RpS3	37532.27778	-	0.820479333	0.000241225
FBgn0031636	:CG12194	148.3718039	+	10.34271432	0.000241225
FBgn0011272	:Rpl13	36538.32389	-	0.827891158	0.000253708
FBgn0031872	:ihog	975.5337338	+	1.316065356	0.000253708
FBgn0019957	:ND-42	2562.842812	-	0.89705739	0.000319403
FBgn0039713	:RpS8	52054.9528	-	0.819244025	0.000319403
FBgn0036752	:Adgf-A	567.4870746	-	0.706966901	0.000349614
FBgn0264979	:CG4267	1290.724805	-	0.780251837	0.000367555
FBgn0034756	:Cyp6d2	75.61459267	-	0.448575352	0.000387945
FBgn0001079	:fu	1142.865532	+	1.250370041	0.00039137
FBgn0014026	:Rpl7A	54352.67161	-	0.835237603	0.000416611
FBgn0016926	:Pino	2915.989298	-	0.768673663	0.000416611
FBgn0283451	:br	783.3306672	-	0.637538375	0.000416611
FBgn0033713	:CG8841	1718.525663	+	1.287027289	0.000429179
FBgn0003274	:RpLP2	35732.36386	-	0.78688401	0.000471726

FlyBase ID	geneSymbol	basemean	direction	foldchange	adjpvalue
FBgn0004374	neb	939.2500737	+	1.190758273	0.00047752
FBgn0037661	Ada	176.7782883	+	1.399212177	0.000516786
FBgn0038769	Regnase-1	545.5313994	+	1.211194495	0.000522461
FBgn0031536	Cog3	960.6399184	+	1.162466062	0.000532717
FBgn0033486	dmpd	2476.584623	+	1.115842944	0.000534468
FBgn0040388	boi	1931.979768	+	1.181468991	0.000554993
FBgn0026409	Mpcp2	14220.5233	-	0.899296328	0.000604815
FBgn0011284	RpS4	45584.3079	-	0.870622953	0.000614942
FBgn0023549	Mct1	865.3475219	-	0.785833778	0.000614942
FBgn0034968	Rpl12	27721.90915	-	0.837205744	0.000614942
FBgn0052318	CG32318	468.2089764	+	1.249691557	0.000614942
FBgn0032329	Art8	402.2596693	-	0.825218715	0.000620413
FBgn0032407	Pex19	1033.871649	-	0.883434789	0.000620413
FBgn0039883	RhoGAP100F	251.3897917	-	0.727361319	0.000637409
FBgn0030049	Trf4-1	5669.012768	+	1.179548395	0.000638355
FBgn0002932	neur	1337.904465	+	1.173492477	0.000645301
FBgn0050295	lpk1	462.6543251	+	1.345720909	0.000645301
FBgn0061476	Zwilch	1320.879797	+	1.133928567	0.000645301
FBgn0261274	Ero1L	1934.067374	+	1.159906044	0.000645301
FBgn0026433	Grip128	2742.512102	+	1.121947334	0.000761662
FBgn0030055	Rubicon	902.0240532	+	1.246515474	0.000812542
FBgn0030183	CG15309	878.9950907	-	0.813856815	0.000812542
FBgn0026326	Mad1	1816.028742	+	1.115107141	0.000848017
FBgn0029117	Surf1	662.5545355	-	0.831348417	0.000848017
FBgn0036058	CG6707	4212.763079	-	0.884558553	0.000863249
FBgn0261610	CG42699	622.4560875	+	1.200068822	0.000863249
FBgn0039359	Rpl27	25854.7212	-	0.820669103	0.000871519
FBgn0086758	chinmo	20.97222256	-	0.358029753	0.000879112
FBgn0015396	jumu	4642.846909	+	1.169785103	0.000917973
FBgn0017577	Mcm5	5736.909004	+	1.102011091	0.000917973
FBgn0029785	Rpl35	27285.84965	-	0.846217049	0.000917973
FBgn0038183	CG9286	527.2678154	-	0.726916397	0.000917973
FBgn0263863	mRpl45	1569.909157	-	0.897779059	0.001048462
FBgn0004387	Klp98A	2324.495471	+	1.156970195	0.001085722
FBgn0036104	CG6418	1738.309408	+	1.121673301	0.001103549
FBgn0022023	eIF3h	8583.111919	-	0.85509825	0.001129877
FBgn0034345	CG5174	3864.404029	-	0.889561282	0.001129877
FBgn0266719	stac	578.1833799	-	0.792699648	0.001129877
FBgn0027535	botv	681.996975	+	1.249521889	0.001159658
FBgn0001168	h	410.555571	-	0.745300819	0.001161219
FBgn0024183	vig	2002.621601	-	0.794076924	0.001168557
FBgn0000566	Eip55E	2975.889767	-	0.898370277	0.001172301
FBgn0029897	RpL17	30956.003	-	0.844775149	0.001189818
FBgn0037351	RpL13A	41384.17259	-	0.821543691	0.001189818
FBgn0259734	Nost	5138.227893	+	1.133160457	0.001202894
FBgn0022774	Oat	979.1555107	-	0.638821751	0.001232758
FBgn0015568	alpha-Est1	1026.919698	-	0.840210222	0.001248903
FBgn0031191	Cp110	949.4486791	+	1.136892372	0.001248903
FBgn0035295	Cnb	997.3728529	+	1.207081864	0.001248903
FBgn0262511	Vha44	6126.717925	-	0.883920656	0.001248903
FBgn0031741	CG11034	713.1122099	+	1.480485077	0.001315054
FBgn0001108	DCTN1-p150	3884.902471	+	1.154298948	0.001315332
FBgn0261602	Rpl8	45585.81545	-	0.851149646	0.001315332
FBgn0027509	TBCD	1744.438678	+	1.168312215	0.001327127
FBgn0034354	GstE11	462.7030045	-	0.624147429	0.001327127
FBgn0063449	Uhg2	428.4680393	-	0.705495524	0.001327127
FBgn0010412	RpS19a	32602.93213	-	0.841274351	0.001387714
FBgn0036754	CG5589	970.0702746	-	0.84509796	0.001503303
FBgn0027518	Wdr24	1402.816531	+	1.131323003	0.00151001

FlyBase ID	geneSymbol	basemean	direction	foldchange	adjpvalue
FBgn0033916	Usp20-33	2338.30703	+	1.171598794	0.00151001
FBgn0035753	Rpl18	29401.4621	-	0.862041758	0.001544894
FBgn0033845	mars	3932.594771	+	1.218103621	0.001622738
FBgn0032864	CG2493	2746.569421	-	0.885267504	0.001654831
FBgn0035308	CG15822	190.2593163	-	0.613526441	0.001654831
FBgn0041171	ago	8992.464292	+	1.160017815	0.001654831
FBgn0039830	ATPsynC	41469.69623	-	0.914533493	0.00166247
FBgn0051365	CG31365	1971.730095	+	1.134013816	0.001664724
FBgn0083123	Uhg5	485.2261552	-	0.666708201	0.001664724
FBgn0000575	emc	1577.615472	-	0.841272992	0.001664858
FBgn0033607	CG9062	3084.720219	+	1.101494525	0.001687855
FBgn0030466	CG15744	1688.148915	+	1.219645206	0.00170644
FBgn0005533	RpS17	29709.87854	-	0.836462694	0.001727715
FBgn0027082	ProRS-m	350.1077659	-	0.823205329	0.001733311
FBgn0037027	HIPP1	4411.795183	+	1.127285262	0.001733311
FBgn0052579	CG32579	854.0948718	+	1.584823512	0.001733311
FBgn0267977	mh	1072.278068	+	1.15213279	0.001733311
FBgn0284408	trol	4155.81645	-	0.716108173	0.001733311
FBgn0005593	Rpl7	42614.35909	-	0.858676804	0.001738468
FBgn0053113	Rtnl1	8058.894185	-	0.912220729	0.001738468
FBgn0004406	tam	927.0921888	+	1.240309289	0.001776989
FBgn0261954	east	9764.440786	+	1.256520879	0.001776989
FBgn0010280	Taf4	5987.543558	+	1.19224923	0.001778392
FBgn0030268	Klp10A	7560.368945	+	1.182963779	0.001806714
FBgn0030581	Cg14408	1402.008036	+	1.145102792	0.001806714
FBgn0038427	ema	1820.288191	+	1.120761398	0.001874053
FBgn001124	Got1	3685.282998	+	1.093624902	0.001880426
FBgn0002924	ncd	2838.245162	+	1.155098141	0.002104094
FBgn0034712	Alp8	193.8766782	-	0.039723832	0.002104094
FBgn0261647	Axud1	1805.828215	+	1.201006859	0.002113692
FBgn0264542	hwt	56.7796716	-	0.581633883	0.002145185
FBgn0265487	mbl	319.1742455	-	0.73008429	0.002145185
FBgn0033836	CG18278	887.235666	+	1.111344065	0.002198685
FBgn0029912	CG4557	1102.113967	+	1.2242031	0.002201249
FBgn0065047	snoRNA:U3:54Ab	34.52251795	-	0.435471305	0.002214652
FBgn0265276	(I3)neo38	402.6438447	-	0.681405201	0.002221994
FBgn0030228	BTBD9	1678.404635	+	1.425492053	0.002227587
FBgn0004397	Vinc	2758.608417	+	1.12780258	0.002265265
FBgn0010409	Rpl18A	40720.01919	-	0.853137284	0.002265265
FBgn0052745	CR32745	69.41458209	+	2.024332015	0.002265265
FBgn0039857	Rpl6	45536.24732	-	0.872275578	0.00231829
FBgn0034606	ASPP	332.9325991	-	0.758932155	0.002427088
FBgn0034618	CG9485	3320.213882	+	1.148720565	0.002427088
FBgn0027567	CG8108	9473.665141	+	1.164121302	0.002456964
FBgn0010226	GstS1	3212.543142	-	0.879014745	0.002467626
FBgn0053051	CG33051	361.421034	-	0.797212171	0.002479135
FBgn0010265	Rps13	29873.06532	-	0.862517185	0.002540904
FBgn0020618	Rack1	55266.75459	-	0.865243855	0.002540904
FBgn0021874	Nle	534.8105597	-	0.793751896	0.002540904
FBgn0029799	CG15772	92.06893531	-	0.051718814	0.002540904
FBgn0032453	CG6180	4916.80032	-	0.853845725	0.002540904
FBgn0035388	CG2162	3633.324759	+	1.198146699	0.002540904
FBgn0037716	Son	2031.130948	+	1.182222768	0.002540904
FBgn0036053	IPLA2-VIA	4117.339605	-	0.904509441	0.002549698
FBgn0266671	Sec6	873.796953	+	1.183679131	0.002549698
FBgn0026372	Rpl23A	59681.01146	-	0.872746246	0.002654831
FBgn0261597	Rps26	36212.59218	-	0.839102232	0.002654831
FBgn0261850	Xpd	1309.485695	+	1.112483316	0.002654831
FBgn0262531	CG43085	29.12064225	+	9.522095731	0.002654831

FlyBase ID	geneSymbol	basemean	direction	foldchange	adjpvalue
FBgn0030500	Ndc80	1414.609349	+	1.148751779	0.002715628
FBgn0031606	CG15439	1973.007154	+	1.223758664	0.002838192
FBgn0263864	Dark	751.7192942	-	0.801420599	0.002858635
FBgn0010217	ATPsynbeta	29693.88534	-	0.86438893	0.002941426
FBgn0020647	KrT95D	1894.635049	+	1.122252023	0.003122959
FBgn0037581	CG7352	74.10096256	+	1.537830911	0.003122959
FBgn0028387	chm	1849.511335	+	1.160152552	0.003164696
FBgn0039631	Sirt7	766.9148277	+	1.169844975	0.003176737
FBgn0032195	CG4908	629.9292757	-	0.873219468	0.003180441
FBgn0034058	Pex11	1201.95323	-	0.782180076	0.003198567
FBgn0000520	dwg	730.1392772	+	1.185581312	0.003217354
FBgn0004404	RpS14b	11915.33293	-	0.835578856	0.003217354
FBgn0030099	CG12056	162.7435904	-	0.748403396	0.003217354
FBgn0086694	Bre1	4746.679225	+	1.145015322	0.003217354
FBgn0000158	bam	989.1503105	+	1.353928999	0.003274091
FBgn0262719	CG43163	49.76003594	-	0.164217193	0.003314561
FBgn0025366	lp259	6329.577174	-	0.745805151	0.003340452
FBgn0052103	SCaMC	3644.063035	+	1.100922967	0.003340452
FBgn0266457	lncRNA:CR45082	45.67602264	-	0.588516784	0.003340452
FBgn0037109	MED1	4255.608681	+	1.138615485	0.003477918
FBgn0027364	Six4	400.7674107	-	0.700880513	0.003539869
FBgn0052576	CG32576	242.3785237	-	0.75839648	0.003539869
FBgn0263113	Cc2d2a	36.22765813	+	4.923374464	0.003580536
FBgn0037354	CG12171	1323.546514	-	0.874501969	0.003638011
FBgn0035997	phol	4677.738529	+	1.161476569	0.003638045
FBgn0003292	rt	1085.598473	+	1.189888649	0.003805199
FBgn0261823	Asx	2536.127911	+	1.216069566	0.003857497
FBgn0031696	Bub1	2579.953026	+	1.216621814	0.003894723
FBgn0041182	Tep2	712.4588406	-	0.529265435	0.003919043
FBgn0010078	Rpl23	34881.2185	-	0.82966054	0.003931104
FBgn0030048	CG12112	1410.156719	+	1.788883125	0.003931104
FBgn0032154	mtDNA-helicase	990.5583805	+	1.118121824	0.003931104
FBgn0032481	CG16972	2190.865219	+	1.255703067	0.003931104
FBgn0035849	ERR	770.9235404	+	1.136546352	0.003931104
FBgn0015926	dah	2665.116027	+	1.178396317	0.003946431
FBgn0037899	Rpl24-like	5050.786483	-	0.853762629	0.003946431
FBgn0001139	gro	6871.874222	+	1.132962621	0.003952548
FBgn0035422	Rpl28	26286.88736	-	0.865500057	0.003961168
FBgn0267795	Frl	2053.427503	+	1.135377518	0.003961168
FBgn0051224	CG31224	6007.551328	+	1.20549029	0.003998827
FBgn0065048	snoRNA:U3:54Aa	33.536555029	-	0.429094235	0.004057788
FBgn0037020	Pex14	1722.478195	-	0.900469729	0.004118444
FBgn0035533	Cip4	2263.120523	+	1.106711965	0.004149202
FBgn0000964	tj	1660.787174	-	0.635252794	0.004174565
FBgn0024991	CG2694	3016.462852	+	1.11834688	0.004174565
FBgn0030718	ND-20	1921.616762	-	0.897310556	0.004174565
FBgn0259791	bora	1826.50405	+	1.185875094	0.004174565
FBgn0262559	Mdh2	9084.888374	-	0.898882868	0.004197544
FBgn0034053	Cyp4aa1	57.91083411	-	0.499884039	0.004216606
FBgn0037612	CG8112	1232.427314	+	1.176541929	0.004225582
FBgn0003089	pip	82.96068887	-	0.579131172	0.004230381
FBgn0086908	egg	2280.93798	+	1.129237386	0.00429372
FBgn0033428	Urod	1833.232834	-	0.865072624	0.004307529
FBgn0002542	lds	4936.598647	+	1.090156311	0.004337291
FBgn0030847	CG12991	326.1897575	-	0.765655771	0.004524882
FBgn0013756	Mtor	11527.56159	+	1.154780973	0.004562599
FBgn0036825	Rpl26	30531.51926	-	0.845296645	0.004562599
FBgn0015296	Shc	1420.159692	+	1.103144747	0.004620365
FBgn0260750	Mulk	823.4249387	-	0.862913998	0.004647685

FlyBase ID	geneSymbol	basemean	direction	foldchange	adjpvalue
FBgn0051216	Naam	261.7596562	-	0.761159502	0.004665362
FBgn0011774	lrbp	1928.211697	+	1.104763983	0.004675206
FBgn0023407	B4	3514.845687	+	1.127998108	0.004704011
FBgn0261859	CG42788	1161.113041	+	1.199639363	0.004704011
FBgn0003598	Su(var)3-7	6499.961379	+	1.151966385	0.00473876
FBgn0010441	bli	1056.512427	+	1.152435863	0.004752385
FBgn0022786	Hira	2145.923331	+	1.112365935	0.004752385
FBgn0030060	CG2004	1640.108692	+	1.131636344	0.004752385
FBgn0031703	CG12512	491.1621771	+	1.312084764	0.004752385
FBgn0033608	CG13220	1212.414409	-	0.858314484	0.004752385
FBgn0285950	Rpl19	49094.98741	-	0.846459794	0.004752385
FBgn0003301	rut	498.6599647	+	1.247498751	0.004776758
FBgn0030242	sofe	1792.131535	+	1.099546265	0.004831649
FBgn0035541	CG15019	1527.024304	-	0.84809587	0.004831649
FBgn0037723	SpdS	1557.246262	-	0.855905376	0.004831649
FBgn0039508	CG3368	1696.990516	+	1.109759489	0.004831649
FBgn0050020	CG30020	3362.976812	+	1.174418134	0.004831649
FBgn0261584	CG42694	91.16679353	-	0.598397346	0.004831649
FBgn0267913	lncRNA:CR46194	87.21429769	-	0.660481775	0.004831649
FBgn0021906	RFeSP	4025.987671	-	0.884890442	0.004894732
FBgn0035374	mRpS35	1307.659849	-	0.887361017	0.00493824
FBgn0260997	CG42598	101.4941211	-	0.528145284	0.005022587
FBgn0038168	omd	1843.0103	+	1.199359552	0.005088845
FBgn0034243	Ns2	2285.818059	-	0.853138051	0.005180212
FBgn0039241	CG11089	2122.746781	-	0.889548658	0.005290267
FBgn0015756	Rpl9	30098.69159	-	0.850170227	0.005305995
FBgn0285948	Rpl27A	39817.085	-	0.842868253	0.005337524
FBgn0027506	EDTP	4214.521671	+	1.145300488	0.005453889
FBgn0030241	feo	5112.586967	+	1.152532886	0.005453889
FBgn0033555	RpS15Ab	4568.84011	-	0.839426971	0.005541421
FBgn0029174	Fkbp59	5701.452192	-	0.885448099	0.005668228
FBgn0267967	corolla	188.3017466	+	1.413814095	0.005727866
FBgn0035807	CG7492	2216.557815	+	1.143804957	0.005735967
FBgn0083027	snoRNA:Psi18S-531	184.3220705	-	0.766096811	0.005759015
FBgn0285947	Rps10b	28792.49042	-	0.852468177	0.005759015
FBgn0034722	Rtf1	3475.607781	+	1.134700845	0.005777659
FBgn0265297	pabp	43616.44898	-	0.837634523	0.005798566
FBgn0005278	Sam-S	13329.91131	-	0.850186247	0.005896813
FBgn0030631	CG6227	1949.654018	+	1.174405364	0.005896813
FBgn0036927	Gabat	5145.258385	-	0.88074046	0.005896813
FBgn0037715	CG9399	996.9718364	+	1.165453636	0.005896813
FBgn0038244	CG7987	4616.349331	+	1.145241557	0.005896813
FBgn0002891	DNApol-zeta	1275.731381	+	1.174607575	0.005899307
FBgn0011606	Klp3A	3981.256566	+	1.106746946	0.005899307
FBgn0030894	Mvb12	2227.172017	+	1.070278235	0.005899307
FBgn0034743	RpS16	24773.06923	-	0.849455956	0.005899307
FBgn0267534	asRNA:CR45874	317.6200882	-	0.71222326	0.005899307
FBgn0011703	RnrL	11267.7868	+	1.083033132	0.005945769
FBgn0013548	(l2)dtl	3538.510953	+	1.147909368	0.005945769
FBgn0036844	Mkp3	2530.247664	+	1.140323264	0.005945769
FBgn0038834	Rps30	24761.45217	-	0.848407673	0.006001881
FBgn0036257	RhoGAP68F	2456.527607	+	1.085117866	0.006117417
FBgn0022768	Pp2C1	4361.565232	+	1.249353257	0.00614418
FBgn0026179	siz	1969.875573	+	1.171590305	0.00614418
FBgn0032499	Uvrag	753.117761	+	1.193868777	0.00614418
FBgn0037327	PEK	4159.427721	+	1.146895891	0.00614418
FBgn0032079	CG31886	847.0551516	+	1.232140345	0.0061568
FBgn0029709	CHOp24	1913.819432	-	0.880348473	0.006177813
FBgn0037328	RpL35A	26310.77346	-	0.855141636	0.006177813

FlyBase ID	geneSymbol	basemean	direction	foldchange	adjpvalue
FBgn0010356	Taf5	1230.173	+	1.130623209	0.006301682
FBgn0003279	Rpl4	63123.99868	-	0.869561299	0.006341176
FBgn0260935	Vps15	661.2681129	+	1.196399144	0.006388987
FBgn0262619	DNAlig1	3037.866979	+	1.090515983	0.006388987
FBgn0033548	CG7637	801.7353587	-	0.772029891	0.006399695
FBgn0002626	Rpl32	27192.148	-	0.860097746	0.006478288
FBgn0027889	ball	3471.661258	+	1.113672746	0.006478288
FBgn0033749	achi	425.4845342	-	0.801218104	0.006478288
FBgn0034425	CG11906	1065.757826	+	1.11399095	0.006478288
FBgn0085599	Cg41284	96.32892969	-	0.525140114	0.006478288
FBgn0261238	Alh	4553.519287	+	1.162450149	0.006619204
FBgn0028525	c(2)M	851.6765142	-	0.813300729	0.006874888
FBgn0036620	CG4842	484.7503781	+	2.224894962	0.006913228
FBgn0038853	RhoGAP93B	2318.845804	+	1.192298522	0.006913228
FBgn0011818	oaf	3214.135343	-	0.790859214	0.007048784
FBgn0000064	Ald1	8023.930013	-	0.914671362	0.00711598
FBgn0000449	dib	25.27254143	-	0.548525366	0.00711598
FBgn0030616	Rpl37a	34973.15251	-	0.868959539	0.00711598
FBgn0033699	Rps11	29635.969	-	0.851976315	0.00711598
FBgn0039909	ND-49	2807.427979	-	0.902480841	0.00711598
FBgn0045800	Uhg1	569.1899605	-	0.695697996	0.00711598
FBgn0261609	elf2alpha	5440.306151	-	0.915804914	0.00711598
FBgn0016984	sktl	4572.472109	+	1.181875971	0.007180844
FBgn0010173	Rpa-70	7466.071717	+	1.098684595	0.007211336
FBgn0086698	frtz	812.9295965	+	1.258850118	0.007256456
FBgn0039767	CG2218	2666.033974	+	1.196355944	0.007270532
FBgn0264001	bru3	58.77272457	-	0.644161197	0.007270532
FBgn0000524	dx	4038.4765	+	1.136076367	0.007413625
FBgn0038473	Ns1	2953.001096	-	0.845972887	0.007413625
FBgn0055386	ash1	4243.237182	+	1.196359261	0.00750421
FBgn0039016	Dcr-1	2194.201927	+	1.152366182	0.00758709
FBgn0013325	Rpl11	23834.44506	-	0.856648005	0.007724537
FBgn0027291	Idh3a	5960.627064	-	0.886748338	0.007724537
FBgn0029093	cathD	7971.354232	-	0.868903762	0.007724537
FBgn0010408	Rps9	23860.93004	-	0.849345825	0.007736499
FBgn0261984	lre1	1988.47015	+	1.183860987	0.007736499
FBgn0001612	Grip91	2477.111177	+	1.116080989	0.007754736
FBgn0003079	Raf	2105.293315	+	1.122477255	0.007796566
FBgn0032666	CG5758	80.39257375	-	0.590654612	0.007796566
FBgn0261278	grp	8219.492082	+	1.062581437	0.007808985
FBgn0003464	sol	3655.460285	+	1.189248599	0.00788842
FBgn0023531	CG32809	572.3487869	+	1.361806367	0.007966482
FBgn0037339	Pi4KIIalpha	2326.496569	+	1.089891497	0.007966482
FBgn0027611	LManII	2407.314297	-	0.774687562	0.007997866
FBgn0029148	NHP2	1667.702737	-	0.861847002	0.007997866
FBgn0016694	Pdp1	978.5894356	-	0.773324504	0.008018946
FBgn0033649	pyr	240.6061506	-	0.706934512	0.008124767
FBgn0034138	Rps15	35831.35435	-	0.848085612	0.008152818
FBgn0027500	spd-2	7507.362679	+	1.15530739	0.008175348
FBgn0030853	ND-24	1901.897588	-	0.905374898	0.008193562
FBgn0050054	CG30054	245.8909725	-	0.697068275	0.008288463
FBgn0002441	I(3)mbt	2711.98254	+	1.23186619	0.008296283
FBgn0028833	Dak1	2030.002056	-	0.899972079	0.008296283
FBgn0260632	dl	3510.848967	+	1.09672715	0.008296283
FBgn0261053	Cad86C	125.2176497	-	0.659231053	0.008307064
FBgn0010382	CycE	10252.27474	+	1.180566259	0.008319962
FBgn0039697	CG7834	3393.057369	-	0.930066159	0.008397328
FBgn0001297	kay	1172.196418	-	0.847865191	0.008456505
FBgn0003656	swns	5544.962197	+	1.174764242	0.00853405

FlyBase ID	geneSymbol	basemean	direction	foldchange	adjpvalue
FBgn0028931	CG16863	162.196824	+	1.295779661	0.00853405
FBgn0039757	RpS7	47544.12217	-	0.860136559	0.008549238
FBgn0034753	CG2852	18400.39802	-	0.88227469	0.008620931
FBgn0265298	SC35	1861.82447	-	0.856161185	0.008620931
FBgn0027785	NP15.6	1586.034549	-	0.882419192	0.00880165
FBgn0034570	CG10543	3266.438596	+	1.227284434	0.00880165
FBgn0000721	for	8556.689126	+	1.122854438	0.008820209
FBgn0027660	blot	3274.5488	+	1.195655713	0.008847042
FBgn0029715	CG11444	3866.57837	-	0.907358919	0.008847042
FBgn0034576	ND-B14.7	1225.191845	-	0.874041704	0.008847042
FBgn0034788	CG13532	6.07834644	-	0.070433728	0.008847042
FBgn0035033	CG3548	1539.989297	+	1.151520143	0.008847042
FBgn0043458	CG12084	2263.85501	+	1.134549474	0.008847042
FBgn0038251	Hexim	1646.21059	+	1.088306535	0.008877021
FBgn0002552	lin	2501.545134	+	1.218509347	0.008950163
FBgn0031759	lid	7734.291339	+	1.192674443	0.008950163
FBgn0035769	CTCF	2026.201136	+	1.116477329	0.008950163
FBgn0004403	RpS14a	18473.9292	-	0.840063241	0.009088487
FBgn0034075	Asph	625.4515704	-	0.539535121	0.009088487
FBgn0037671	ATP6AP2	4326.163329	-	0.901345239	0.009192543
FBgn0261596	RpS24	34962.9426	-	0.855594279	0.009202075
FBgn0260441	RpS12	24646.9166	-	0.848970382	0.009333132
FBgn0261573	CoRest	5249.936549	+	1.091470594	0.009386482
FBgn0029838	CG4666	334.0660813	-	0.66609312	0.009481383
FBgn0001234	lncRNA:Hsromega	913.648165	-	0.721521892	0.009494554
FBgn0036213	Rpl10Ab	21815.3119	-	0.843916146	0.009622911
FBgn0000635	Fas2	696.9234039	-	0.794502902	0.009675148
FBgn0010194	Wnt5	760.2555026	+	1.251396534	0.009841605
FBgn0031016	kek5	1730.666167	+	1.201771761	0.00984239
FBgn0035229	pns	3253.821774	+	1.211951908	0.00984239
FBgn0053526	PNUTS	3922.346908	+	1.163680296	0.009916986
FBgn0038826	Syp	572.9453092	-	0.713063824	0.010119188
FBgn0011204	cue	6822.201579	+	1.126018217	0.010144607
FBgn0016696	PitsIre	5081.816426	+	1.161169126	0.010144607
FBgn0031474	CG2991	1350.226779	+	1.135314856	0.010305628
FBgn0001308	Khc	6535.387034	+	1.119976271	0.010331854
FBgn0037525	CG17816	499.6076051	-	0.794522412	0.010331854
FBgn002593	RpLP1	39411.56383	-	0.839019131	0.010358074
FBgn0034599	hng1	463.5093764	+	1.153516459	0.010358074
FBgn0035726	CG9953	5656.378206	-	0.815020741	0.010385452
FBgn0270924	zf30C	3255.42713	+	1.103863897	0.010464612
FBgn0260479	CG31904	42.42961265	-	0.552214958	0.010536761
FBgn0266083	ocm	2178.462522	+	1.23414091	0.01057758
FBgn0001180	hb	2896.502236	+	1.226594771	0.010655074
FBgn0004583	ex	605.803016	-	0.768600012	0.010655074
FBgn0031052	Elys	3466.999464	+	1.21344858	0.010655074
FBgn0037371	Sym	2348.533998	+	1.090854305	0.010655074
FBgn0010342	Map60	4440.958394	+	1.141512386	0.010782861
FBgn0000318	cl	2065.23074	-	0.907551067	0.010848884
FBgn0015295	Shark	1603.928034	+	1.153054807	0.010878387
FBgn0002783	mor	7821.71309	+	1.199513547	0.011081134
FBgn0027095	Manf	2481.64603	-	0.909948434	0.011124786
FBgn0035026	Fcp1	2150.423811	+	1.129742519	0.011124786
FBgn0085385	bma	32.37813256	+	37.8686235	0.011124786
FBgn0267910	lncRNA:CR34335	783.1465136	-	0.786220975	0.011124786
FBgn0004368	Ptp4E	2282.934197	+	1.179540122	0.01120329
FBgn0033473	CG12128	1914.181579	-	0.892237539	0.01120612
FBgn0020621	Pkn	3211.143738	+	1.139450673	0.011227564
FBgn0283450	Glo1	2193.098276	-	0.896649453	0.011310301

FlyBase ID	geneSymbol	basemean	direction	foldchange	adjpvalue
FBgn0015615	:SMC3	3681.858155	+	1.122998609	0.011443228
FBgn0086695	:hd	1750.265206	+	1.170426099	0.011443228
FBgn0261794	:kcc	1095.728927	+	1.147392611	0.011443228
FBgn0011655	:Med	2035.971221	+	1.184896693	0.011582047
FBgn0028697	:RpL15	29361.89835	-	0.839251884	0.011695306
FBgn0262114	:RanBPM	5416.064836	+	1.125050943	0.011695306
FBgn0030877	:Arp8	1288.03222	+	1.092807823	0.011715241
FBgn0032295	:CG12299	2374.225065	+	1.180287437	0.01174396
FBgn0011020	:Sas-4	2091.28019	+	1.128617417	0.011770616
FBgn0030687	:RpIIIc160	1147.077175	+	1.097028728	0.011770616
FBgn0034390	:CG15093	2072.073186	-	0.885778012	0.01179272
FBgn0040475	:SH3PX1	1731.562636	+	1.127834102	0.011868832
FBgn0261608	:RpL37A	15986.71616	-	0.841507952	0.011871751
FBgn0004643	:Zw10	3131.318043	+	1.13134186	0.011895339
FBgn0035254	:CG7974	749.4539096	-	0.727813824	0.011912889
FBgn0261532	:cdm	2096.638433	+	1.163069662	0.011967042
FBgn0032821	:CdGAPr	2489.624097	+	1.247010918	0.011975799
FBgn0015509	:Cul1	12345.6402	+	1.074722361	0.011980939
FBgn0027548	:nito	4897.050109	+	1.150707457	0.011980939
FBgn0032138	:CG4364	8779.570226	-	0.897032187	0.011980939
FBgn0038746	:Surf6	2777.626292	-	0.919593052	0.011980939
FBgn0042092	:CG13773	1513.229627	-	0.892462262	0.011980939
FBgn0044452	:Atg2	2088.547464	+	1.124256811	0.011980939
FBgn0035896	:CG6983	1094.457783	-	0.787924437	0.012288068
FBgn0029689	:Cg6428	677.9572012	+	1.155025543	0.012309762
FBgn0003545	:sub	2204.022434	+	1.096986966	0.012339434
FBgn0041096	:rols	144.2515495	-	0.738296595	0.012339434
FBgn0267351	:Topors	2027.376167	+	1.22972145	0.012347469
FBgn0030701	:CG16952	2455.265032	+	1.121235836	0.012559378
FBgn0014269	:prod	1577.43539	+	1.097470138	0.012648846
FBgn0015834	:elf3i	6188.834775	-	0.915338141	0.012648846
FBgn0020272	:mst	997.2328568	+	1.144194219	0.012648846
FBgn0025633	:CG13366	10106.59946	+	1.165824116	0.012648846
FBgn0032717	:CG10600	3997.112236	+	1.197357526	0.012648846
FBgn0033752	:CG8569	983.3744588	+	1.111298359	0.012648846
FBgn0035036	:CG4707	835.887565	+	1.121281633	0.012648846
FBgn0000543	:ecd	1114.979569	+	1.147663188	0.012688965
FBgn0028956	:mthl3	162.6045975	-	0.713508478	0.012800572
FBgn0028497	:CG3530	1195.66713	+	1.161285859	0.012837872
FBgn0086710	:RpL30	18130.72821	-	0.840532163	0.012877779
FBgn0259697	:nvd	43.47934772	-	0.435735816	0.012928794
FBgn0262714	:Sap130	2244.450555	+	1.191373542	0.012970858
FBgn0005642	:wdn	3368.622691	+	1.138382256	0.012983036
FBgn0013764	:Chi	2559.039845	+	1.124315946	0.013066568
FBgn0002031	:I(2)37Cc	5831.233253	-	0.918885776	0.013354795
FBgn0259212	:cno	7964.040087	+	1.166302134	0.013354795
FBgn0025815	:Mcm6	3957.695295	+	1.136988208	0.013405727
FBgn0085443	:spri	3709.123449	+	1.11796877	0.013412797
FBgn0260991	:Incenp	4807.745723	+	1.154176925	0.013412797
FBgn0021895	:ytr	4229.419453	-	0.907141152	0.013522862
FBgn0029756	:CG3309	994.5333832	+	1.119550396	0.013575398
FBgn0000250	:cact	9395.575592	+	1.117754112	0.013588566
FBgn0032228	:CG5367	249.5634521	-	0.693335714	0.013810903
FBgn0027335	:Rip11	4504.912433	+	1.124691109	0.013811585
FBgn0022344	:CG10340	1038.906211	-	0.886092566	0.013834876
FBgn0033225	:TTLL12	1035.496037	-	0.860170983	0.013866514
FBgn0261592	:RpS6	38910.52686	-	0.865351766	0.013891228
FBgn0031814	:retrm	963.0364147	+	1.172590111	0.013920001
FBgn0037744	:Mpi	585.6991853	-	0.825376022	0.013962253

FlyBase ID	geneSymbol	basemean	direction	foldchange	adjpvalue
FBgn0033915	CG8485	2870.424438	+	1.126378503	0.014077482
FBgn0011785	BRWD3	6005.443304	+	1.19790155	0.01409169
FBgn0085789	CR41506	46.76401388	-	0.590956199	0.014131342
FBgn0037686	Rpl34b	21327.64739	-	0.843298352	0.014153846
FBgn0040234	c12.2	681.4557294	+	1.221730383	0.014165265
FBgn0026575	hang	9299.058603	+	1.200917739	0.014166774
FBgn0027504	CG8878	3973.557868	+	1.103479413	0.014166774
FBgn0036489	CG7011	951.2486199	-	0.902814364	0.014193899
FBgn0067102	GlcT	1796.254226	+	1.177655907	0.014193899
FBgn0052772	Cg32772	2765.978646	+	1.118077723	0.014266578
FBgn0039407	CG14544	409.8712802	-	0.869847787	0.014365339
FBgn0259238	CG42336	1057.410029	-	0.831568681	0.014365339
FBgn0003942	RpS27A	27964.74346	-	0.847273121	0.014438943
FBgn0038640	CG7706	1153.50154	+	1.107782073	0.014438943
FBgn0027342	fz4	2248.115376	+	1.105549576	0.014459443
FBgn0030878	CG6769	1157.011733	-	0.889342419	0.014528574
FBgn0004860	ph-d	1488.204501	+	1.193174038	0.014574624
FBgn0015268	Nap1	29672.67053	-	0.884701291	0.014574624
FBgn0015288	Rpl22	18103.68691	-	0.880379401	0.014618638
FBgn0036299	Tsf2	2177.658845	+	1.09075691	0.014713704
FBgn0038145	Droj2	18742.7907	+	1.114653413	0.0148652
FBgn0262473	Tl	9473.577719	+	1.153793469	0.0148652
FBgn0026598	Apc2	2334.162951	+	1.156016972	0.014992377
FBgn0002878	mus101	2063.429753	+	1.178955494	0.015003194
FBgn0034113	Cg8060	891.744868	+	1.149093562	0.015026407
FBgn0031194	CG17598	2080.280017	+	1.074157174	0.015112895
FBgn0000256	capu	1457.409631	+	1.192153144	0.015370167
FBgn0038478	cal1	5141.463828	+	1.097041693	0.015370167
FBgn0003268	rod	3052.551244	+	1.102920913	0.015455061
FBgn0010411	RpS18	26345.93126	-	0.853515452	0.015455061
FBgn0022069	Nnp-1	4089.468119	-	0.926101803	0.015455061
FBgn0022724	Taf8	1151.920049	+	1.126129828	0.015455061
FBgn0034527	CG9945	1556.490359	+	1.103917547	0.015455061
FBgn0036368	CG10738	155.5108583	+	1.511843629	0.015455061
FBgn0052529	Hers	1575.537577	+	1.17724645	0.015455061
FBgn0053523	CG33523	1981.565751	-	0.92358337	0.015455061
FBgn0261599	RpS29	34820.48189	-	0.864124646	0.015455061
FBgn0264326	DNApol-epsilon255	2402.617967	+	1.146529167	0.015455061
FBgn0265767	zyd	1952.191286	-	0.900099429	0.015455061
FBgn0283536	Vha13	9579.463618	-	0.919318839	0.015455061
FBgn0285949	Rpl31	30521.45799	-	0.861197021	0.015455061
FBgn0267912	CanA-14F	6427.14936	+	1.143797973	0.01545633
FBgn0037655	Kcmf1	5652.511954	+	1.086901866	0.015542046
FBgn0003015	osk	33891.85676	-	0.875888233	0.015665111
FBgn0013765	cnn	4122.050596	+	1.125508007	0.015665111
FBgn0030087	CG7766	3511.074837	+	1.178690959	0.015799492
FBgn0085212	CG34183	273.1855768	-	0.801253565	0.015799492
FBgn0266916	Cenp-C	4719.399316	+	1.16920207	0.015836548
FBgn0003575	su(sable)	2373.629148	+	1.169170035	0.01584224
FBgn0031118	RhoGAP19D	3057.356248	+	1.206413071	0.01584224
FBgn0022935	D19A	1695.309026	+	1.154128837	0.0158899
FBgn0029930	CG12541	11.66302448	-	0.404269592	0.0158899
FBgn0036373	Tgi	1326.672549	+	1.122937487	0.0158899
FBgn0041150	hoe1	3385.009137	+	1.119984243	0.0158899
FBgn0015803	RtGEF	1640.872008	+	1.142319996	0.015908926
FBgn0030093	Bap111	6708.233469	+	1.173326599	0.015908926
FBgn0038418	pad	1127.163169	+	1.220955409	0.015908926
FBgn0039696	Rnb	1455.05631	+	1.131726541	0.015908926
FBgn0029893	CG14442	6160.261483	+	1.176706702	0.015955319

FlyBase ID	geneSymbol	basemean	direction	foldchange	adjpvalue
FBgn0031488	Ccdc85	141.5323707	-	0.67405937	0.016081536
FBgn0031745	rau	149.7111937	-	0.73888127	0.016081536
FBgn0044046	Ilp7	100.1727097	+	1.350582326	0.016081536
FBgn0283494	Adk2	5113.619183	-	0.873789309	0.016081536
FBgn0010300	brat	9820.897072	+	1.17176063	0.016096707
FBgn0033317	CG8635	4064.931008	-	0.907281822	0.016096707
FBgn0034059	CG8320	680.4943439	-	0.835967072	0.016096707
FBgn0034796	CG3700	423.5336788	-	0.864069272	0.016096707
FBgn0035488	CG11593	2329.047396	+	1.092614129	0.016096707
FBgn0047038	ND-13B	1155.693791	-	0.835564585	0.016096707
FBgn0052296	Mrtf	3014.671606	+	1.167461343	0.016096707
FBgn0264324	spg	1999.476185	+	1.171967565	0.016290902
FBgn0010198	RpS15Aa	29367.80347	-	0.850592069	0.016398459
FBgn0261963	mid	204.5317173	-	0.702320841	0.016398459
FBgn0266911	asRNA:CR45371	9.650964323	-	0.240995436	0.016479401
FBgn0004390	RasGAP1	3533.154173	+	1.136591622	0.016917397
FBgn0052638	CG32638	841.3471474	+	1.143578075	0.016991567
FBgn0085397	Fili	21.58846067	-	0.471127956	0.016991567
FBgn0264406	dysc	17.00241828	-	0.463352512	0.016991567
FBgn0029840	raptor	3471.011866	+	1.168955599	0.017033391
FBgn0035437	Strip	2003.666732	+	1.116409123	0.017073379
FBgn0004868	Gdi	8473.86411	-	0.811145041	0.017114487
FBgn0034491	Hsl	2480.389531	+	1.190896619	0.017209985
FBgn0037760	FBXO11	4809.00415	+	1.192644611	0.017209985
FBgn0030759	CG13014	397.1084104	-	0.844038113	0.017287556
FBgn0004636	Rap1	5336.436287	-	0.904189148	0.017317092
FBgn0030243	CG2186	2358.697265	+	1.217342765	0.017317092
FBgn0085376	CG34347	401.1730227	-	0.705286486	0.017362365
FBgn0024733	RpL10	28593.06722	-	0.87077415	0.017604776
FBgn0003941	RpL40	27975.4635	-	0.890174984	0.017628193
FBgn0013531	MED20	736.6502466	+	1.254708045	0.017652299
FBgn0087011	CG41520	22.75910481	-	0.410516562	0.017652299
FBgn0260634	eIF4G2	4886.797049	+	1.207883742	0.017652299
FBgn0038290	CG6912	26.88151226	+	5.430507942	0.017725351
FBgn0027525	LTV1	4292.216921	-	0.860253583	0.017893328
FBgn0039993	CG17691	2441.219278	-	0.872357875	0.017962434
FBgn0034564	CG9344	637.2329737	-	0.843435355	0.018054474
FBgn0037623	CG9801	466.6903397	+	1.214537476	0.018151486
FBgn0035397	PAN3	6710.318609	+	1.262930847	0.018210041
FBgn0032454	Cg5787	3569.531068	+	1.132524908	0.018239153
FBgn0038872	Nelf-A	4155.256015	+	1.180415153	0.018239153
FBgn0025455	CycT	6177.765675	+	1.201132498	0.018255751
FBgn0261786	mi	3564.299281	+	1.131476623	0.018286856
FBgn0033890	Ctf4	2376.208123	+	1.156281876	0.018390973
FBgn0030010	CG10959	803.7474969	+	1.116128699	0.018391281
FBgn0036916	Mtr3	738.6534924	-	0.891476643	0.018391281
FBgn0002413	dco	8618.128281	+	1.144418522	0.018440698
FBgn0003360	sesB	43507.62936	-	0.879819592	0.018468365
FBgn0063494	GstE6	2246.010388	-	0.736991979	0.018468365
FBgn0032346	Csl4	793.1467609	-	0.860988431	0.018532036
FBgn0032600	BuGZ	2523.568687	-	0.925189579	0.018532036
FBgn0033912	RpS23	33684.13887	-	0.86044302	0.018532036
FBgn0035827	Srp9	1507.237963	-	0.895744346	0.018532036
FBgn0031830	COX5B	3230.014055	-	0.889602878	0.018723328
FBgn0037720	CG8312	1637.930627	+	1.172536476	0.018723328
FBgn0027579	mino	3328.662147	+	1.120975587	0.018727095
FBgn0035393	CG16753	845.7495503	-	0.851496684	0.018727095
FBgn0037944	CG6923	2248.736101	+	1.244788431	0.018727095
FBgn0038277	RpS5b	22468.24268	-	0.778824886	0.018727095

FlyBase ID	geneSymbol	basemean	direction	foldchange	adjpvalue
FBgn0000043	:Act42A	8607.872878	-	0.888089052	0.018745333
FBgn0025186	:ari-2	2400.448289	+	1.154068071	0.018745333
FBgn0029970	:Nek2	1530.733664	+	1.150538325	0.018745333
FBgn0035237	:CG13917	5701.851649	+	1.155028601	0.018745333
FBgn0042138	:CG18815	2665.706705	-	0.906986244	0.018745333
FBgn0086904	:Nacalpha	23290.8776	-	0.864741542	0.018752494
FBgn0039406	:RpL34a	5973.643673	-	0.884026511	0.01904536
FBgn0032167	:CG5853	655.9063585	-	0.754603453	0.019161443
FBgn0000559	:eEF2	134418.681	-	0.914360794	0.019292028
FBgn0023081	:gek	2580.251245	+	1.09188609	0.019304377
FBgn0052205	:hpRNA:CR32205	1389.141747	-	0.859045237	0.019304377
FBgn0039632	:Cul5	2285.640314	+	1.134549562	0.019332993
FBgn0261383	:IntS6	3004.643963	+	1.138500251	0.019332993
FBgn0000212	:brm	5407.849613	+	1.19233502	0.019423383
FBgn0039555	:mRps22	1436.222868	-	0.90517428	0.019423383
FBgn0265512	:mlt	2016.238045	-	0.855555514	0.019606891
FBgn0030293	:CG1737	5708.670751	+	1.105981613	0.01965031
FBgn0046225	:CG17230	570.1406128	+	1.173815538	0.01965031
FBgn0029693	:CG6379	769.1785668	+	1.140148939	0.019925624
FBgn0035953	:CG5087	1445.637056	+	1.113433198	0.019925624
FBgn0019624	:COX5A	5561.986149	-	0.889198705	0.020303653
FBgn0004856	:Bx42	3044.002172	+	1.091222594	0.020312226
FBgn0031939	:CG13796	94.44276112	-	0.674019267	0.020318652
FBgn0035099	:CG6845	166.9381737	-	0.781834539	0.020373274
FBgn0024998	:CG2685	1684.610653	+	1.103435128	0.020810181
FBgn0052212	:CG32212	8.631296731	-	0.412259306	0.020849887
FBgn0026441	:mal	1146.515914	+	1.090440346	0.021018557
FBgn0026441	:ear	2367.843998	+	1.136977145	0.021018557
FBgn0052226	:Pex23	1057.44728	+	1.205429276	0.021018557
FBgn0285952	:eEF5	26025.11587	-	0.834448543	0.021018557
FBgn0027348	:bgm	5047.061431	+	1.116066782	0.021044771
FBgn0014391	:sun	3141.123972	-	0.873742139	0.021102192
FBgn0036450	:Tdrd3	2334.73994	+	1.101079494	0.021383246
FBgn0044324	:Chro	5218.203168	+	1.102237449	0.021383246
FBgn0031698	:Ncoa6	6375.289159	+	1.202881211	0.0213841
FBgn0020887	:Su(z)12	3476.833109	+	1.149332349	0.02141575
FBgn0037734	:trbd	1164.300272	+	1.130979982	0.02141575
FBgn0263998	:Ack-like	3021.122045	+	1.096848188	0.02141575
FBgn0035957	:CG5144	107.1892035	+	1.663615811	0.021607809
FBgn0028572	:qtc	272.32825	-	0.720205111	0.021880377
FBgn0019938	:Rpl1	3513.251479	-	0.859290298	0.021960499
FBgn0039169	:Spps	1417.801801	+	1.244919624	0.021961753
FBgn0259993	:lncRNA:CR42491	271.1093052	-	0.657183769	0.021961753
FBgn0260484	:HIP	6766.60843	-	0.918436597	0.021961753
FBgn0261703	:gce	458.0590313	-	0.793068705	0.021961753
FBgn0000489	:Pka-C3	731.2308933	-	0.732249468	0.02196242
FBgn0014133	:bif	14070.98499	+	1.200330898	0.02196242
FBgn0037555	:Ada2b	4447.83806	+	1.090108073	0.02196242
FBgn0012058	:Cdc27	3672.417781	+	1.122008328	0.021963019
FBgn0014388	:sty	378.5235045	-	0.661753736	0.021963019
FBgn0030834	:CG8675	1175.338007	-	0.888764813	0.021963019
FBgn0037315	:Cerk	1739.357446	+	1.086274237	0.021963019
FBgn0266752	:lncRNA:CR45225	20.34081641	+	2.056996538	0.021963019
FBgn0025743	:mbt	3787.502357	+	1.16028092	0.022059226
FBgn0027610	:Dic1	931.8475049	-	0.835729027	0.022059226
FBgn0052666	:Drak	3213.422229	+	1.132849122	0.022059226
FBgn0016754	:sba	1244.576874	+	1.172289863	0.02209987
FBgn0038860	:ice2	828.9781307	+	1.159193495	0.02209987
FBgn0005536	:Mbs	4298.84058	+	1.143721512	0.022103696

FlyBase ID	geneSymbol	basemean	direction	foldchange	adjpvalue
FBgn0037779	CG12811	842.2747196	-	0.861239454	0.022104463
FBgn0036772	CG5290	920.9850203	-	0.863630547	0.022176643
FBgn0037093	Cdk12	3821.139961	+	1.164198364	0.02218811
FBgn0032261	CG6094	491.1221156	-	0.871994536	0.022223722
FBgn0000140	asp	8627.368912	+	1.11234822	0.022227405
FBgn0028974	xmas	2168.096896	+	1.149430625	0.022227405
FBgn0036062	CG6685	861.3556951	+	1.201803153	0.022227405
FBgn0036165	chrb	6092.008162	+	1.149934908	0.022227405
FBgn0037759	CG8526	102.3552637	+	1.392795246	0.022252843
FBgn0031062	Cg14230	1773.261585	+	1.122264394	0.022529801
FBgn0030812	wcy	6726.68703	+	1.159572254	0.022530418
FBgn0036004	Jarid2	9007.652395	+	1.234497646	0.022530418
FBgn0029763	Usp16-45	5838.772116	+	1.17275018	0.022696293
FBgn0032987	RpL21	34544.31647	-	0.859448456	0.022723171
FBgn0020385	pug	623.1039545	+	1.23816439	0.022745716
FBgn0029082	hbs	11.6949151	-	0.316558117	0.022745716
FBgn0037025	Spc105R	3430.253214	+	1.144816818	0.022745716
FBgn0004861	ph-p	682.5210926	+	1.216077503	0.023274522
FBgn0019936	Rps20	26204.90987	-	0.874289034	0.023274522
FBgn0000032	Acph-1	2840.446203	-	0.930627493	0.023283146
FBgn0039668	Trc8	2011.526421	+	1.148112302	0.023283146
FBgn0005666	bt	708.8477694	-	0.682880614	0.023595487
FBgn0004795	retn	8104.038865	+	1.174555879	0.023800904
FBgn0011817	nmo	3218.763582	+	1.144054624	0.023915567
FBgn0027490	D12	1285.374269	+	1.100034901	0.023915567
FBgn0033485	RplP0-like	1632.230073	-	0.856586822	0.023915567
FBgn0050183	CG30183	3148.52283	+	1.166406089	0.023915567
FBgn0262527	nsl1	6315.489625	+	1.111465952	0.023915567
FBgn0259745	wech	8796.542464	+	1.132672918	0.023923891
FBgn0050438	Ugt50B3	88.55988474	-	0.643258732	0.023973218
FBgn0265669	CG44476	42.8196117	-	0.604100778	0.023973218
FBgn0267488	Mcr	4870.573279	+	1.124594104	0.024003544
FBgn0034061	Ufc1	557.8136989	-	0.849802262	0.024044457
FBgn0037305	CG12173	955.5341363	-	0.85408501	0.024045899
FBgn0039559	NSD	8375.508624	+	1.168504619	0.024045899
FBgn0283724	Girdin	4622.81427	+	1.1683614	0.024045899
FBgn0027783	SMC2	3710.165355	+	1.075575239	0.024105705
FBgn0000463	DL	2715.005795	+	1.155933748	0.024116392
FBgn0030311	CG11699	850.7498326	-	0.895277647	0.024120744
FBgn0011740	alpha-Man-IIa	1541.535744	+	1.164189163	0.024189048
FBgn0010328	woc	10004.17881	+	1.193085309	0.024298654
FBgn0016041	Tom40	8213.255678	-	0.912044299	0.024298654
FBgn0036801	MYPT-75D	2668.956117	+	1.152545804	0.024300509
FBgn0260049	flr	4358.746446	+	1.092901939	0.024300509
FBgn0262686	CG43156	27.00092879	-	0.452852426	0.024300509
FBgn0085400	side-V	188.2734656	-	0.661050084	0.024364086
FBgn0003462	Sod1	6747.085857	-	0.913657638	0.0244403478
FBgn0035771	Sec63	3938.44869	+	1.129376549	0.024584104
FBgn0028484	Ack	1556.297661	+	1.177039071	0.024636082
FBgn0037874	Ttcp	38463.42401	-	0.834104158	0.024722727
FBgn0034214	CG6550	535.6310027	-	0.84503634	0.024809631
FBgn0000283	Cp190	8865.020234	+	1.146623337	0.024953139
FBgn0041087	wun2	2380.323018	+	1.087996124	0.025035564
FBgn0261016	clos	7324.708728	-	0.86619552	0.025274004
FBgn0019644	ATPsynB	4348.706112	-	0.886573889	0.025278178
FBgn0030136	Rps28b	23618.48202	-	0.87626727	0.025278178
FBgn0036557	mRpS31	1196.070309	-	0.873393171	0.025278178
FBgn0037270	eIF3f1	6037.124918	-	0.910341137	0.025278178
FBgn0053124	CG33124	43.1146501	+	324.0111035	0.025278178

FlyBase ID	geneSymbol	basemean	direction	foldchange	adjpvalue
FBgn0260874	Ir76a	133.5421213	-	0.521163517	0.025278178
FBgn0261836	Msp300	1371.359159	-	0.793448626	0.025278178
FBgn0283659	THG	347.9992363	-	0.871679398	0.025278178
FBgn0039084	CG10175	89.47848979	-	0.679790637	0.025400902
FBgn0034259	P32	4762.941694	-	0.894040775	0.025519525
FBgn0033813	fsd	309.4661374	-	0.845361743	0.025529694
FBgn0260397	Su(var)3-3	1993.614731	+	1.133145876	0.025922225
FBgn0020235	ATPsyn gamma	5957.706823	-	0.897459922	0.026001127
FBgn0034186	CG8950	843.035687	+	1.130618602	0.026254862
FBgn0026059	Mhcl	2222.29442	+	1.153609915	0.026332702
FBgn0039863	Cg1815	3166.924468	+	1.173278108	0.026332702
FBgn0034590	Magi	1615.535796	+	1.163706479	0.026356199
FBgn0261570	raskol	5053.72602	+	1.164738928	0.026356199
FBgn0004432	Cyp1	33489.58945	-	0.914755197	0.026472667
FBgn0014184	Oda	14445.59054	-	0.88657295	0.026500833
FBgn0003210	rb	2928.68619	+	1.11725392	0.026530438
FBgn0262167	ana1	2337.91361	+	1.205746429	0.026592771
FBgn0010909	msn	6176.962562	+	1.11038965	0.026810181
FBgn0016726	Rpl29	14219.84349	-	0.847409432	0.026810181
FBgn0031055	et	10.54107119	+	3.142245049	0.02689777
FBgn0260959	MCPH1	4136.191357	+	1.133870013	0.027017199
FBgn0032229	ClpP	1369.833334	-	0.890355514	0.027082612
FBgn0039338	XNP	4521.365483	+	1.130757682	0.027082998
FBgn0050372	Asap	2585.72719	+	1.143818227	0.027082998
FBgn0016685	Nlp	13057.23032	-	0.923102874	0.027128814
FBgn0035600	Cyt-c1	4568.728482	-	0.913881184	0.027128814
FBgn0039419	CG12290	146.7058442	-	0.71471136	0.027161193
FBgn0026679	IntS4	1227.154581	+	1.192184486	0.027180382
FBgn0086129	snama	3385.876075	+	1.110349153	0.027275608
FBgn0030530	jub	2023.745096	+	1.177609351	0.027295608
FBgn0032198	eEF1delta	7788.715246	-	0.902575662	0.027295608
FBgn0034816	CG3085	126.5845185	-	0.471805859	0.027295608
FBgn0037026	CG3634	1172.665005	+	1.164758035	0.027295608
FBgn0003557	Su(dx)	4034.824726	+	1.136980137	0.027355834
FBgn0039300	Rps27	18859.72871	-	0.868013847	0.027355834
FBgn0014037	Su(Tpl)	8125.480657	+	1.141122899	0.027443188
FBgn0035206	sturkopf	1539.836975	-	0.821280978	0.027443188
FBgn0023508	Ocrl	2261.611515	+	1.156299994	0.027556349
FBgn0030361	CG1492	285.3673192	+	1.200023953	0.027556349
FBgn0263077	CG43340	2704.60058	+	1.168029026	0.027625407
FBgn0010213	Sod2	3872.971126	-	0.916124114	0.027672441
FBgn0030685	Graf	3494.976992	+	1.093321703	0.027672441
FBgn0030839	CG5613	273.6956154	+	1.184676722	0.027672441
FBgn0036660	CG13025	2006.583971	+	1.086358427	0.027672441
FBgn0001257	ImpL2	2299.523634	-	0.779190221	0.027767563
FBgn0039927	CG11155	173.3572524	-	0.750461067	0.027767563
FBgn0026878	CG4325	36.9258663	-	0.627127233	0.027781084
FBgn0031980	Rpl36A	23523.44822	-	0.848433361	0.027781084
FBgn0037708	CG9386	198.8597184	-	0.832855823	0.027781084
FBgn0259683	Ir40a	53.61085012	-	0.410308023	0.028254249
FBgn0036842	Ugt316A1	2065.019529	+	1.141396121	0.028408111
FBgn0261625	GLS	1276.682036	-	0.833388195	0.028672405
FBgn0039150	CG13605	1255.342737	+	1.110405497	0.028777892
FBgn0000499	dsh	2424.51295	+	1.095752321	0.028812672
FBgn0036684	CG3764	1869.739625	+	1.124698142	0.028812672
FBgn0036921	RhoGDI	4329.319065	-	0.903809338	0.028812672
FBgn0034117	CG7997	951.908417	+	1.110426784	0.028963801
FBgn0027508	Tnks	1721.28259	+	1.164079716	0.028966229
FBgn0028962	AlaRS-m	960.0083387	+	1.12979232	0.028966229

FlyBase ID	geneSymbol	basemean	direction	foldchange	adjpvalue
FBgn0032161	CG4594	582.6571176	-	0.656250282	0.028966229
FBgn0034724	babos	678.9622975	-	0.667802571	0.028966229
FBgn0039654	Brd8	1149.96976	+	1.139568142	0.028966229
FBgn0035232	CG12099	2127.452568	-	0.930814885	0.028966945
FBgn0000181	bic	40913.52632	-	0.893231823	0.0290078
FBgn0027615	OXA1L	1764.606291	+	1.082369961	0.029196025
FBgn0028982	Spt6	4768.024299	+	1.193790321	0.029196194
FBgn0024329	Mekk1	4065.491634	+	1.17885838	0.029371849
FBgn0030858	IntS2	1570.376909	+	1.122954177	0.029409226
FBgn0033538	Cg11883	1181.908239	-	0.917009017	0.029409226
FBgn0039348	Npl4	3911.293465	+	1.088822689	0.029409226
FBgn0261385	scra	4995.780279	+	1.193245322	0.029409226
FBgn0002044	swm	5993.247021	+	1.135353203	0.02942977
FBgn0027601	pdgy	2227.673808	+	1.133689078	0.02942977
FBgn0086662	snoRNA::Psi28S-3186	16.17703891	-	0.548747226	0.029436367
FBgn0264384	lncRNA::CR43836	516.9549161	+	1.486921055	0.029436367
FBgn0025388	CG12179	2216.301157	+	1.19916517	0.029443276
FBgn0035699	CG13300	23.6466412	-	0.599579987	0.029443276
FBgn0052594	be	951.8419047	+	1.160519096	0.029532173
FBgn0039492	CG6051	3425.907504	+	1.139654679	0.029707433
FBgn0020388	Gcn5	1895.232565	+	1.079941578	0.029764038
FBgn0043900	pygo	5827.489036	+	1.12824079	0.029791959
FBgn0086855	CG17078	3380.950904	+	1.090070429	0.029846835
FBgn0010113	hdc	4577.070009	+	1.142901778	0.029930343
FBgn0082831	pps	4748.878892	+	1.160475616	0.029930343
FBgn0031459	HINT1	2689.902576	-	0.905895756	0.029938668
FBgn0034553	CG9993	18.35449415	+	16.80165587	0.029938668
FBgn0035617	I(3)psg2	3644.182257	+	1.169376305	0.029938668
FBgn0039112	SdhD	1374.313293	-	0.902575044	0.029938668
FBgn0051262	CG31262	1244.069065	-	0.829113593	0.029938668
FBgn0053267	CG33267	5.876753587	-	0.328065053	0.029938668
FBgn0064225	Rpl5	47215.09298	-	0.858885806	0.029938668
FBgn0265988	mv	2038.309271	+	1.134829488	0.029938668
FBgn0001169	H	4798.259572	+	1.133389434	0.02994694
FBgn0003278	Rpl135	1464.832138	-	0.846427723	0.02994694
FBgn0051547	NKCC	84.06714554	+	2.6389746	0.02994694
FBgn0000414	Dab	2556.393879	+	1.204674564	0.029951993
FBgn0004859	ci	314.6122714	-	0.697752676	0.029977713
FBgn0036662	CG9706	777.6934959	-	0.916044157	0.030147018
FBgn0030630	CG12608	1632.986483	-	0.91172847	0.030212072
FBgn0034915	elf6	2113.012727	-	0.909938708	0.030521901
FBgn0250850	rig	6349.461588	+	1.078739727	0.030521901
FBgn0259481	Mob2	2088.421331	+	1.093430662	0.030626949
FBgn0039125	Ndc1	1624.276123	+	1.104236772	0.030691536
FBgn0259832	CG34229	128.0776295	-	0.78932162	0.03074012
FBgn0029006	Smurf	4722.031904	+	1.13047855	0.031240392
FBgn0032018	CG7806	1758.299632	+	1.128979019	0.031240392
FBgn0262866	S6klI	937.5407572	+	1.115733441	0.031299684
FBgn0283510	Pal1	2074.167261	+	1.107645081	0.031299684
FBgn0261938	mtRNAPol	1585.139942	+	1.11807162	0.031305345
FBgn0038390	Rbf2	2213.898884	+	1.122522499	0.031617287
FBgn0012051	CalpA	574.5828839	-	0.793548628	0.031883448
FBgn0021760	chb	4073.686177	+	1.143424261	0.031883448
FBgn0025879	Timp	338.3482507	-	0.760433246	0.032101901
FBgn0033716	Den1	1356.653297	-	0.881615434	0.032264641
FBgn0010905	Spn	6248.038769	+	1.192839377	0.032288539
FBgn0030720	CG8939	2803.486269	-	0.91632893	0.03254627
FBgn0039688	Kul	94.19988323	-	0.721931361	0.032685638
FBgn0020278	loco	1281.410055	+	1.167910055	0.03306575

FlyBase ID	geneSymbol	basemean	direction	foldchange	adjpvalue
FBgn0030274	Lint-1	1120.427077	+	1.095563539	0.03306575
FBgn0001989	ND-B17	1200.062724	-	0.899651867	0.033184963
FBgn0004379	Klp67A	2864.162325	+	1.118326544	0.033184963
FBgn0017558	Pdk	2908.741937	+	1.101959673	0.033184963
FBgn0017579	RpL14	30067.64842	-	0.867654026	0.033184963
FBgn0020510	Abi	2754.054324	+	1.089422848	0.033184963
FBgn0030958	CR6900	19.77869078	-	0.462690211	0.033184963
FBgn0031051	Ranbp21	4100.796022	+	1.184442561	0.033184963
FBgn0033155	Br140	4294.563396	+	1.188493609	0.033184963
FBgn0033929	Tfb1	2327.408637	+	1.07226155	0.033184963
FBgn0039636	Atg14	738.7083854	+	1.085985737	0.033184963
FBgn0039846	PNPase	904.7090658	+	1.132191482	0.033184963
FBgn0250786	Chd1	7292.115476	+	1.156566565	0.033184963
FBgn0260469	CR14578	936.3766232	+	1.194640409	0.033184963
FBgn0285917	sbb	7868.380566	+	1.224590173	0.033184963
FBgn0035298	SCOT	759.6463672	+	1.137049492	0.033299814
FBgn0037073	Tsr1	3906.098181	-	0.90934166	0.033321513
FBgn0000592	Est-6	23.88359697	-	0.304996066	0.033454969
FBgn0032430	CG6388	662.3901657	-	0.862361178	0.033454969
FBgn0037358	elm	2254.454368	-	0.897737921	0.033454969
FBgn0010228	HmgZ	1030.990841	-	0.752862541	0.033575339
FBgn0032479	CG16974	6688.103353	+	1.106661735	0.033595259
FBgn0023513	CG14803	1683.40013	+	1.13534006	0.033658268
FBgn0033784	SCCRO3	1597.832001	+	1.117474722	0.033671351
FBgn0047000	CG33946	8.461578188	-	0.403006968	0.033874297
FBgn0039459	IntS12	755.7793794	+	1.139386045	0.034102942
FBgn0039227	polybromo	5336.764054	+	1.13911107	0.034280318
FBgn0027609	orgue	834.0047048	+	1.12719853	0.034357076
FBgn0031820	Daxx	5847.92967	+	1.145817048	0.034357076
FBgn0027080	TyrRS	3143.150046	-	0.908460178	0.034472811
FBgn0011739	wts	3877.375281	+	1.159517965	0.034618969
FBgn0029861	CG3815	2111.787395	+	1.158974626	0.034742689
FBgn0030710	CG8924	3004.04783	+	1.100668343	0.034742689
FBgn0034976	CG4049	2453.058161	+	1.148078326	0.034742689
FBgn0035791	CG8539	103.1272468	-	0.696725825	0.034742689
FBgn0000927	f(1)Ya	7810.609964	+	1.103459457	0.034788637
FBgn0034964	IntS1	3362.249688	+	1.121771046	0.034788637
FBgn0038065	Snx3	2768.119841	-	0.951308234	0.034788637
FBgn0022343	CG3760	4564.072638	-	0.909384638	0.034903089
FBgn0025373	Fpps	1790.886884	+	1.208201689	0.034903089
FBgn0029506	Tsp42Ee	4200.275841	-	0.803826535	0.034903089
FBgn0031008	CG8010	1774.405738	-	0.855424187	0.034903089
FBgn0034365	CG5335	656.7940498	-	0.838441691	0.034903089
FBgn0262582	cic	7693.562025	+	1.182306158	0.034903089
FBgn0038840	Grik	9.748233105	-	0.394783032	0.03499701
FBgn0035900	ZC3H3	324.406972	+	1.181325683	0.035299521
FBgn0031573	CG3407	1050.639087	+	1.130261684	0.035439512
FBgn0025885	Inos	2476.525798	-	0.908731498	0.035677753
FBgn0027868	Nup107	2460.8354	+	1.12331846	0.035677753
FBgn0030787	CG9609	2264.418806	+	1.117623457	0.035677753
FBgn0085434	NaCP60E	275.9317745	-	0.827962704	0.035677753
FBgn0284254	Impbeta11	1717.255315	+	1.164577041	0.035677753
FBgn0038476	kuk	10088.06814	+	1.113805222	0.03587609
FBgn0019637	Atu	1724.755334	+	1.134414867	0.035923327
FBgn0002579	Rpl36	30188.0288	-	0.842605765	0.035955285
FBgn0034008	CG8152	867.2735288	+	1.576556134	0.035955285
FBgn0002906	Blm	2755.742281	+	1.131316519	0.036034735
FBgn0010591	Sply	2142.507068	+	1.081457477	0.036242765
FBgn0017482	T3dh	66.4119198	-	0.71567847	0.036242765

FlyBase ID	geneSymbol	basemean	direction	foldchange	adjpvalue
FBgn0033376	CG8777	608.5931221	-	0.892880754	0.036242765
FBgn0046214	vig2	24099.8654	-	0.932495537	0.036242765
FBgn0263706	CG43658	2299.724852	+	1.19963772	0.036242765
FBgn0036814	CG14073	3689.904636	+	1.192139572	0.036376012
FBgn0002887	mus201	1542.000584	+	1.115614408	0.036404006
FBgn0031377	CG15356	2970.122142	+	1.186768416	0.036404006
FBgn0032796	CG10188	2302.080802	+	1.1740535	0.036404006
FBgn0033092	Rpp25	989.6373515	-	0.903264488	0.036404006
FBgn0264693	ens	7439.79315	+	1.105995997	0.036404006
FBgn0028953	CG14478	7783.128113	+	1.145995514	0.036426431
FBgn0261988	Gprk2	2481.698843	+	1.139667446	0.036440954
FBgn0261854	aPKC	3407.743988	+	1.127719984	0.03647827
FBgn0036537	CG18081	3259.218152	-	0.862219693	0.036673793
FBgn0264950	asRNA:CR44119	20.96469232	-	0.517332832	0.03672477
FBgn0052250	PMP34	1263.552212	+	1.096893085	0.036803897
FBgn0036544	ssf	122.998686	-	0.657652307	0.036935599
FBgn0264984	lncRNA:CR44135	17.03694942	-	0.470846004	0.036935599
FBgn0262732	mbf1	6349.040665	-	0.894105405	0.036965254
FBgn0031381	Npc2a	1926.390151	-	0.887483565	0.036978309
FBgn0040823	dpr6	287.0694854	+	1.488555942	0.036978309
FBgn0004907	14-3-3zeta	16395.24383	-	0.899506945	0.037139748
FBgn0031799	Pez	2599.299375	+	1.14979913	0.037139748
FBgn0034221	CG10764	79.09167782	+	7.84301588	0.037139748
FBgn0036769	Tsp74F	1694.364605	-	0.881660047	0.037139748
FBgn0051619	nolo	31.86116117	-	0.302777496	0.037139748
FBgn0029941	CG1677	8517.965368	+	1.175480135	0.037154789
FBgn0034065	Rrp42	465.4745822	-	0.857805426	0.037154789
FBgn0040212	Dhap-at	954.0929216	+	1.114682853	0.037154789
FBgn0011725	twin	6939.76668	+	1.102724775	0.037255058
FBgn0036334	CG11267	6240.008399	-	0.911510308	0.037255058
FBgn0037918	CG6791	2415.3648	+	1.177326017	0.037255058
FBgn0265778	PDZ-GEF	4263.149457	+	1.149432503	0.037255058
FBgn0021967	ND-PDSW	2395.039972	-	0.903705905	0.037288375
FBgn0000057	adp	1123.348396	+	1.088434687	0.037584445
FBgn0000247	ca	2408.513827	+	1.119643151	0.037628559
FBgn0031886	Nuf2	1105.6119	+	1.15607267	0.037628559
FBgn0031937	CG13795	23.12231648	-	0.398642978	0.037628559
FBgn0034735	CG4610	885.1011234	-	0.798088043	0.037628559
FBgn0262740	Evi5	2158.038088	+	1.113881141	0.037666994
FBgn0003687	Tbp	1603.231515	+	1.084940366	0.037721077
FBgn0015625	CycB3	9438.681471	+	1.10343034	0.037721077
FBgn0023509	mip130	1591.534658	+	1.164065299	0.037721077
FBgn0031630	CG15629	20.42537454	-	0.497209944	0.037721077
FBgn0061200	Nup153	9746.721078	+	1.133015432	0.037721077
FBgn0030506	DNAIg4	571.6661684	+	1.12614864	0.037977419
FBgn0003567	su(Hw)	4594.266264	+	1.111269023	0.038006863
FBgn0003124	polo	12819.52465	+	1.079026678	0.038535363
FBgn0028490	CG31705	1516.141072	-	0.817744642	0.03887904
FBgn0035888	CG7120	392.1748966	-	0.813950368	0.03887904
FBgn0067864	Patj	1788.485531	+	1.132462293	0.03887904
FBgn0263197	Patronin	2690.3342	+	1.160401942	0.03887904
FBgn0003071	Pfk	2732.26619	+	1.167944023	0.039045711
FBgn0025641	DAAM	3129.398084	+	1.185604174	0.039045711
FBgn0030012	CG18262	394.9677225	+	1.14820705	0.039045711
FBgn0027885	cass	3445.293439	-	0.910199744	0.039130052
FBgn0039067	wda	1010.36013	+	1.15336924	0.039130052
FBgn0265002	CG44153	61.72906454	+	1.982649618	0.039130052
FBgn0028343	Ankle2	6720.355663	+	1.118295565	0.039425833
FBgn0030100	CG12106	488.9495568	-	0.883328788	0.039433171

FlyBase ID	geneSymbol	basemean	direction	foldchange	adjpvalue
FBgn0028292	:ric8a	1295.35618	+	1.086085616	0.03943388
FBgn0260004	:Snmp1	52.50061994	-	0.698617065	0.039480562
FBgn0265598	:Bx	793.7071374	+	1.12359937	0.03953833
FBgn0002526	:LanA	2325.815134	-	0.674499293	0.039646486
FBgn0015609	:CadN	271.3667757	-	0.705979915	0.039734665
FBgn0266674	:Sec15	1519.356071	+	1.100311409	0.039734665
FBgn0086444	:l(2)37Cb	751.4377955	+	1.150080101	0.039905741
FBgn0034093	:CG15706	386.1899232	+	1.163026121	0.039915463
FBgn0260945	:Atg1	2708.880371	+	1.129278284	0.039915463
FBgn0039730	:CG7903	918.774625	+	1.172458145	0.03998499
FBgn0039740	:ZIPIC	1030.044834	+	1.104375304	0.03998499
FBgn0034897	:Sesn	3573.627019	+	1.135421451	0.040185054
FBgn0265705	:asRNA:CR44512	52.76484631	-	0.734978106	0.040396171
FBgn0260439	:Pp2A-29B	8958.941711	-	0.950424325	0.040418701
FBgn0003175	:px	3003.521299	+	1.16734169	0.040576118
FBgn0005624	:Psc	1599.993322	+	1.169388135	0.040641698
FBgn0028474	:CG4119	3145.560752	+	1.124669245	0.040641698
FBgn0033375	:CG8078	277.7200179	-	0.830815597	0.040641698
FBgn0034060	:CG8370	2012.901337	+	1.171163669	0.040641698
FBgn0004858	:elB	114.0948371	-	0.768155038	0.040729133
FBgn0034033	:CG8204	285.8026408	-	0.858268309	0.040794632
FBgn0017567	:ND-23	1623.016573	-	0.929201921	0.040896618
FBgn0025582	:elf3e	8968.329685	-	0.899944517	0.040896618
FBgn0033636	:tou	4864.099514	+	1.188783768	0.040963223
FBgn0083120	:Uhg8	169.6012968	-	0.741209445	0.041031434
FBgn0035941	:CG13313	15.0886417	+	3.112713899	0.041069701
FBgn0015521	:RpS21	10119.99511	-	0.855266459	0.041080186
FBgn0037975	:CG3397	104.1603876	-	0.426085128	0.041080186
FBgn0000808	:gd	293.1831975	+	1.152653811	0.041088421
FBgn0034021	:CG8180	10747.58747	+	1.113315704	0.041101801
FBgn0039809	:CG15547	62.45772852	-	0.760934465	0.0411234
FBgn0000416	:Sap-r	21358.37115	-	0.907786121	0.041209845
FBgn0026143	:Cdc45	3305.956936	+	1.112760721	0.041265618
FBgn0031492	:CG3542	2210.643272	+	1.07672876	0.041265618
FBgn0015035	:Cyp4e3	41.61713684	+	3.127748041	0.041373944
FBgn0038569	:CG7218	1866.151528	+	1.069884388	0.041373944
FBgn0001206	:Hmr	2221.650176	+	1.181397705	0.041408435
FBgn0033526	:Caf1-105	3873.594605	+	1.119555447	0.041408435
FBgn0044823	:Spec2	1283.179079	+	1.112549944	0.041408435
FBgn0037489	:Cg1234	2035.310927	-	0.877339912	0.041459428
FBgn0010355	:Taf1	3989.47188	+	1.136226055	0.041491553
FBgn0030738	:CG9915	2821.413481	+	1.082619312	0.041491553
FBgn0031049	:Sec61gamma	2328.403159	-	0.878547449	0.041642175
FBgn0037606	:CG8032	1186.658533	+	1.141369272	0.041642175
FBgn0033085	:CG15908	313.0636406	-	0.850762642	0.041823825
FBgn0263993	:CG43736	5419.478011	+	1.10486162	0.042082329
FBgn0052227	:gogo	7.919286809	+	5.32993623	0.042124571
FBgn0028919	:CG16865	1067.442669	+	1.086996947	0.042207015
FBgn0015277	:Pi3K59F	583.0522927	+	1.152907878	0.042446911
FBgn0266889	:asRNA:CR45350	71.42004405	-	0.673035695	0.042482224
FBgn0039944	:CG17162	175.5797862	-	0.753289494	0.042593314
FBgn0039941	:CG17167	106.2290561	-	0.660256081	0.042908937
FBgn0086707	:ncm	4816.16348	+	1.131912807	0.042922545
FBgn0035772	:Sh3beta	2031.084366	-	0.870561506	0.042982183
FBgn0002719	:Men	5853.642442	+	1.154683168	0.04324827
FBgn0002590	:RpS5a	14977.78842	-	0.869295019	0.043452147
FBgn0029905	:NF-YC	2582.278141	+	1.202757453	0.043452147
FBgn0036624	:RAF2	2760.717358	+	1.125565761	0.043452147
FBgn0041585	:olf186-F	3014.250286	+	1.110088608	0.043452147

FlyBase ID	geneSymbol	basemean	direction	foldchange	adjpvalue
FBgn0053087	LRP1	2331.457246	-	0.798696446	0.043452147
FBgn0259789	zld	9113.8986	+	1.226661141	0.043452147
FBgn0262580	CG43120	28.69296105	+	4.262796555	0.043452147
FBgn0002022	Catsup	1818.811484	-	0.929355424	0.043466691
FBgn0033846	mip120	3254.469979	+	1.101636527	0.043466691
FBgn0037344	CG2926	8395.552368	+	1.149977273	0.043466691
FBgn0013770	Cp1	17754.39222	-	0.855875913	0.043730917
FBgn0032524	Hacd2	807.0087295	-	0.891464497	0.043934905
FBgn0026061	Mipp1	564.1110289	-	0.77747309	0.043942664
FBgn0032793	CG10189	182.6784782	-	0.814249595	0.043942664
FBgn0035032	ATPsymF	5063.833393	-	0.910471442	0.043942664
FBgn0042201	Nplp3	14.28740647	-	0.154485932	0.043942664
FBgn0261446	CG13377	193.2946775	-	0.77121881	0.043942664
FBgn0086784	stmA	1600.459474	+	1.107559105	0.044368559
FBgn0037332	Hcs	1288.377503	+	1.133613928	0.044446891
FBgn0037780	ohgt	980.369797	+	1.080680981	0.044452369
FBgn0051926	CG31926	686.2922735	+	3.427909486	0.044452369
FBgn0028664	VhaM9.7-c	983.7087864	-	0.870318802	0.044543522
FBgn0030481	CG1662	1655.56937	-	0.912035683	0.044543522
FBgn0036515	AIMP2	1686.133533	-	0.92441657	0.044543522
FBgn0264942	lncRNA:CR44111	133.9875468	+	1.7694246	0.044543522
FBgn0003218	rdgB	1981.235588	+	1.172920649	0.044662502
FBgn0027786	Mtch	2644.381196	-	0.906038405	0.044662502
FBgn0034817	Art7	869.3047184	-	0.863123473	0.044662502
FBgn0041111	iili	3597.935581	+	1.14646952	0.044775537
FBgn0030799	CG4872	160.882576	+	1.272314502	0.044779812
FBgn0000352	cos	2403.911765	+	1.104878186	0.044782839
FBgn0003486	spo	102.5628779	-	0.557079513	0.044782839
FBgn0015543	snoRNA:Me28S-A1322	28.73816569	-	0.643346779	0.044782839
FBgn0085437	CG34408	1740.525808	+	1.143910842	0.044782839
FBgn0005638	slbo	30.34285505	-	0.542441941	0.045015208
FBgn0025608	Faf2	3223.008453	+	1.091336996	0.045015208
FBgn0034931	CG2812	50.7153034	-	0.618113999	0.045015208
FBgn0250848	26-29-p	37712.19129	-	0.937419202	0.045015208
FBgn0014861	Mcm2	5590.220238	+	1.069431217	0.04505148
FBgn0031449	CG31689	2677.392856	+	1.129107139	0.04505148
FBgn0035282	CNMa	8.537438226	-	0.452602436	0.04505148
FBgn0036667	kud	445.3620626	-	0.878577164	0.04505148
FBgn0040344	Lztr1	1053.268418	+	1.130731756	0.04505148
FBgn0264785	Hph	3636.006716	+	1.087343248	0.045088037
FBgn0039623	CG1951	2163.652239	+	1.126868153	0.045157242
FBgn0001404	egh	3378.302678	+	1.131041144	0.045551482
FBgn0016794	dos	3368.915263	+	1.073065262	0.045551482
FBgn0035945	CG5026	2243.113697	+	1.08029146	0.045558162
FBgn0004876	cdi	3889.374628	+	1.128644896	0.045601376
FBgn0045063	fdl	1702.310786	+	1.129464562	0.045936067
FBgn0033973	HPS1	268.0424305	+	1.174176152	0.046082639
FBgn0034249	RhoGAP54D	1973.462503	+	1.137381357	0.046184691
FBgn0024277	trio	2378.299275	+	1.168552272	0.046186748
FBgn0051849	CG31849	568.152572	+	1.120490425	0.046186748
FBgn0011763	Dp	6531.37978	+	1.066340213	0.046379823
FBgn0011509	SrpRbeta	1450.890163	-	0.912065621	0.046582075
FBgn0016123	Alp4	1251.559168	-	0.876964439	0.046582075
FBgn0033654	Sobp	160.4964779	-	0.815763086	0.046582075
FBgn0038300	Mau2	1206.383336	+	1.092259255	0.046582075
FBgn0035423	elF1	5360.192035	-	0.870076565	0.046677578
FBgn0002781	mod(mdg4)	16554.15503	+	1.100547343	0.046717021
FBgn0024234	gbg	199.6593818	-	0.739212246	0.046899265
FBgn0004655	wapl	7699.376523	+	1.164893571	0.046927914

FlyBase ID	geneSymbol	basemean	direction	foldchange	adjpvalue
FBgn0039066	EloA	3016.950319	+	1.108845687	0.047248438
FBgn0050055	lncRNA:CR30055	1197.815918	-	0.778964569	0.047271496
FBgn0044323	Cka	2715.50047	+	1.104333955	0.047323686
FBgn0025839	ND-B14.5A	1067.083251	-	0.886641586	0.047350243
FBgn0040087	p115	887.9551742	+	1.122455796	0.047350243
FBgn0265140	Meltrin	2323.321458	+	1.120438813	0.047350243
FBgn0031170	ABCA	1401.915352	+	1.156210427	0.047376131
FBgn0261931	CG42797	2385.709081	+	1.135095614	0.047376131
FBgn0262872	milt	7643.472246	+	1.13591942	0.047376131
FBgn0086384	Mer	2225.278088	+	1.132994959	0.047701679
FBgn0082961	snoRNA:Psi28S-3385b	12.76440449	-	0.521559953	0.047795062
FBgn0264962	Pcf11	3219.269066	+	1.081042007	0.047795062
FBgn0262366	CG43064	27.40939253	+	3.694429996	0.047802646
FBgn0026713	(1)G0007	1548.233703	+	1.141625429	0.047841627
FBgn0030899	Hesr	13.59015517	+	3.038324381	0.047847527
FBgn0035522	CG1273	9.337652593	-	0.425859352	0.047847527
FBgn0032919	CG9253	2905.990327	-	0.923608997	0.047933175
FBgn0041781	SCAR	2451.125478	+	1.09968825	0.047951553
FBgn0004584	Rrp1	2737.144052	+	1.079016388	0.048004773
FBgn0010812	unc-45	986.9899496	+	1.115135454	0.048004773
FBgn0029935	CG4615	1168.633018	+	1.121777787	0.048031426
FBgn0000150	awd	27330.70025	-	0.895422501	0.048180365
FBgn0010222	Nmdmc	431.530846	-	0.846624068	0.048180365
FBgn0031021	ND-18	1411.843504	-	0.912269597	0.048180365
FBgn0039026	CG7029	4142.586391	+	1.114888616	0.048180365
FBgn0032799	CG10166	807.8126224	-	0.909798708	0.048488188
FBgn0043884	mask	14859.11629	+	1.158407338	0.048501003
FBgn0035176	CG13905	107.782224	+	3.04423462	0.048754611
FBgn0011586	e(r)	4314.540305	-	0.787107459	0.048767773
FBgn0024814	Clc	3836.763576	-	0.935456399	0.048767773
FBgn0005648	Pabp2	3069.473295	-	0.907147973	0.049028882
FBgn0016081	fry	2182.728553	+	1.126274092	0.049398635
FBgn0001942	eIF4A	47118.84335	-	0.918977718	0.04955121
FBgn0041174	Vhl	211.6574483	-	0.854947737	0.04955121
FBgn0052582	lncRNA:CR32582	49.90888663	+	3.36038254	0.04955121
FBgn0015360	oxt	1966.427653	+	1.132226651	0.049592473
FBgn0026602	Ady43A	742.1550179	+	1.232112997	0.049668954
FBgn0036958	CG17233	4718.19857	+	1.145591012	0.049830937
FBgn0003345	sd	1427.565303	-	0.811951285	0.049955986
FBgn0031217	CG11377	1643.847281	-	0.928944537	0.049955986
FBgn0032701	CG10341	1088.495584	-	0.884627793	0.049955986
FBgn0038296	CG6752	519.9563056	+	1.419919266	0.049955986

Supplementary Table 3. Differentially expressed genes identified in batch 2. Base mean is the number of transcripts averaged across all samples. “Direction” indicates whether the gene is up- or downregulated. Genes are listed in order of ascending p-values.

FlyBase ID	gene Symbol	base mean	direction	fold change	adj p-value
FBgn0002466	sti	2567.378069	+	1.19986802	0.020965583
FBgn0002878	mus101	1768.938494	+	1.193575101	0.007664678
FBgn0003002	opa	9.940700055	-	0.146821746	0.020965583
FBgn0003009	ord	18.89766649	-	0.259535883	0.000676086
FBgn0003321	sbr	2592.221987	+	1.066857881	0.044449438
FBgn0010039	GstD3	647.4198812	-	0.568860132	0.041371027
FBgn0013548	I(2)dtl	2771.313982	+	1.162424824	0.01488212
FBgn0014076	Vm32E	2212.022724	-	0.584030272	0.026468784
FBgn0014269	prod	1538.285812	+	1.075779139	0.044934776
FBgn0014340	mof	1224.152515	+	1.122737721	0.035597133
FBgn0015558	tty	114.0776161	+	1.976434726	0.010505851
FBgn0015625	CycB3	8620.414521	+	1.122411172	0.020965583
FBgn0020415	ldgf2	1342.315091	-	0.570357933	8.59E-06
FBgn0023083	fray	3238.529366	+	1.151293244	0.02731695
FBgn0024179	wit	274.2822117	-	0.686886595	0.038227561
FBgn0025682	scf	1278.015667	-	0.833133273	0.004494837
FBgn0026876	CG11403	1395.553852	+	1.091437949	0.035597133
FBgn0027539	ili	1504.007043	+	1.163960876	0.040721275
FBgn0027550	CG6495	43.10935962	-	0.558239527	0.041775866
FBgn0027575	GABA-B-R2	67.7039822	-	0.652870695	0.040454554
FBgn0027600	obst-B	111.7877002	-	0.651413815	0.008893075
FBgn0027609	mergue	827.0677602	+	1.130384397	0.010505851
FBgn0028523	CG5888	235.3354953	-	0.813576434	0.042827785
FBgn0028833	Dak1	1929.635699	-	0.915908544	0.041371027
FBgn0029588	CR14798	135.3545458	-	0.643972075	0.000357814
FBgn0029603	CG14053	136.7104089	-	0.750428332	0.022948751
FBgn0029648	CG3603	242.8546079	-	0.675653902	0.000738884
FBgn0029935	CG4615	1053.821009	+	1.117594223	0.035691048
FBgn0030121	Cfp1	1648.536391	+	1.145408285	0.007436248
FBgn0030581	CG14408	1072.008096	+	1.172943585	0.020965583
FBgn0030629	CG9123	582.2233397	-	0.815454093	0.040984151
FBgn0030833	CG8915	1588.612115	+	1.13783515	0.042186298
FBgn0031194	CG17598	1862.573815	+	1.090816691	0.006261432
FBgn0031632	CG15628	37.99669446	-	0.176031504	8.59E-06
FBgn0031717	Oscillin	128.2730167	-	0.68480978	0.031096263
FBgn0032298	CG6724	844.3504586	-	0.793064281	0.01488212
FBgn0032685	CG10211	17.0050028	-	0.227371435	0.029558111
FBgn0033521	CG12896	533.9992717	+	1.234854044	0.023723362
FBgn0033846	mip120	2643.538135	+	1.151767718	0.038227561
FBgn0033900	CysRS-m	396.6680299	-	0.881961655	0.044934776
FBgn0034354	GstE11	386.805883	-	0.674553558	0.035597133
FBgn0034406	Jheh3	744.9666643	-	0.739249646	0.02731695
FBgn0034500	CG11200	613.4689988	-	0.81361021	0.000738884
FBgn0034788	CG13532	21.34791718	-	0.215547216	0.003798563
FBgn0034816	CG3085	188.5217713	-	0.544130786	0.002585338
FBgn0034817	Art7	1048.642378	-	0.862585755	0.036214512
FBgn0034878	pita	2699.596719	+	1.070614904	0.042442423
FBgn0035176	CG13905	215.0185921	-	0.122839904	0.000788237
FBgn0035497	CG14995	779.644	+	1.169576007	0.004690472
FBgn0035769	CTCF	1735.300821	+	1.146828068	0.005665636
FBgn0036330	CG11263	391.723954	-	0.603188588	1.24E-05
FBgn0036476	sstn	631.0573667	+	1.189753928	0.032258376
FBgn0036504	yellow-k	84.82699728	-	0.643434418	0.006333606
FBgn0036640	nxf2	1377.16974	+	1.355934988	8.76E-05
FBgn0036660	CG13025	1857.147246	+	1.083697068	0.035597133
FBgn0036882	CG9279	50.21544236	-	0.519553411	0.039918502
FBgn0037731	CG18542	837.471911	+	1.272618019	0.012972966
FBgn0037853	CG14696	83.65171794	-	0.240231172	0.002234297
FBgn0037975	CG3397	124.6915554	-	0.560269182	0.00117777

FlyBase ID	gene Symbol	base mean	direction	fold change	adj p-value
FBgn0038012	CG10013	39.21599844	-	0.196354197	0.027839429
FBgn0038610	CG7675	422.7594137	-	0.717069509	0.022948751
FBgn0038617	Wdr37	1196.875191	+	1.182786833	8.76E-05
FBgn0038788	Sirt2	371.273389	-	0.792342978	0.02731695
FBgn0038829	CG17271	1777.370688	-	0.885942171	0.04883037
FBgn0039064	CG4467	9.954966297	+	4.861356899	0.046611718
FBgn0039124	tbrd-1	64.16418889	-	0.458288371	0.04913923
FBgn0039419	CG12290	280.199075	-	0.624743231	0.020385505
FBgn0039776	PH4alphaEFB	463.8913252	-	0.689215581	4.80E-05
FBgn0039861	pasha	1261.858753	+	1.111109438	0.041606203
FBgn0040609	CG3348	231.7875563	-	0.697586092	0.044934776
FBgn0041182	Tep2	406.7619766	-	0.569089557	8.59E-06
FBgn0046258	CG12880	226.384431	-	0.590414961	0.006333606
FBgn0046776	CR14033	858.6970133	-	0.676878036	0.000738884
FBgn0050046	CG30046	86.82417057	-	0.523534367	0.007436248
FBgn0050428	CG30428	162.2583737	-	0.564854823	0.033614937
FBgn0051075	CG31075	588.7153676	-	0.762085235	0.034254641
FBgn0051320	HEATR2	335.5975831	-	0.764875617	0.038227561
FBgn0052227	gogo	7.374395931	-	0.203069011	0.045342946
FBgn0052939	CG32939	837.5184617	+	1.272491415	0.012972966
FBgn0083940	RhoU	294.3428639	-	0.801041312	0.043499381
FBgn0085362	Vml	9149.772974	-	0.676067331	0.013734741
FBgn0086758	chinmo	27.75034483	-	0.526363411	0.032924775
FBgn0259791	bora	1824.315804	+	1.127073835	0.02731695
FBgn0260745	mfas	1569.081828	-	0.791124073	0.027839429
FBgn0263510	nclb	1314.64288	-	0.81020839	0.013666629
FBgn0263602	Tasp1	1282.514725	+	1.10350819	0.048225265
FBgn0264077	Cnx14D	7.669855179	-	0.077092993	0.043499381
FBgn0265303	lncRNA:CR44276	15.97006034	-	0.424406226	0.031096263
FBgn0265590	lncRNA:CR44417	234.5636104	-	0.760914467	0.035597133
FBgn0265699	lncRNA:CR44506	60.76908461	+	2.329916361	0.042827785
FBgn0265937	asRNA:CR44724	58.21133897	-	0.616099036	0.011908064
FBgn0266005	lncRNA:CR44779	356.2118844	-	0.778602824	0.022948751
FBgn0266279	lncRNA:CR44964	31.67196191	-	0.113267269	8.59E-06
FBgn0267487	Ptp61F	6164.090579	+	1.092236715	0.007436248
FBgn0267728	otk2	216.844568	+	1.555469078	0.00411407
FBgn0267967	corolla	201.2422042	+	1.375803648	0.044934776

Supplementary Table 4. Differentially expressed genes common to both batch 1 and batch 2. Gene name and summary from FlyBase are provided. Genes with functions related to meiotic or mitotic cell division are highlighted in bold.

Gene Name	GO Terms biological process (Panther)
sticky	intracellular signal transduction ; mitotic cytokinesis ; peptidyl-threonine phosphorylation; regulation of cytokinesis; actomyosin contractile ring assembly ;actomyosin structure organization ;male meiosis cytokinesis; chromatin organization; mitotic cytokinesis
mutagen-sensitive 101	mitotic DNA replication checkpoint; mitotic DNA replication checkpoint ;
lethal-(2)-dentineless	-
proliferation disrupter	rhythm ;
Cyclin B3	;direct assaymitotic cytokinesis ;direct assaymitotic cytokinesis ; mitotic cell cycle phase transition ;
modifier of rpr and grim, ubiquitously expressed	regulation of retinal cell programmed cell death ;non-traceable author statementSCF-dependent proteasomal ubiquitin-dependent protein catabolic process ;sequence modelproteasome-mediated ubiquitin-dependent protein catabolic process; ubiquitin-dependent protein catabolic process ;positive regulation of compound eye retinal cell apoptotic process ; genetic interaction with Diap1
Dak1	pyrimidine nucleotide biosynthetic process ;'de novo' pyrimidine nucleobase biosynthetic process ; nucleobase-containing compound metabolic process
FBgn0029935 -	cytolysis
FBgn0030581 -	intracellular signal transduction ;negative regulation of protein tyrosine kinase activity ;
FBgn0031194	protein dephosphorylation ;positive regulation of pyruvate dehydrogenase activity ;dephosphorylation ;sequence or structural similarity with HGNC:18583
Myb-interacting protein 120	gene amplification ; regulation of transcription, DNA-templated ;determination of adult lifespan ;
Glutathione S transferase E11	glutathione metabolic process ;glutathione metabolic process
FBgn0034788 -	-
FBgn0034816	cilium movement involved in cell motility ;microtubule nucleation
Arginine methyltransferase 7	peptidyl-arginine methylation, to asymmetrical-dimethyl arginine ;sequence or structural similarity with Art1peptidyl-arginine methylation ;
FBgn0035176	-
CTCF	maintenance of rDNA ;direct assayresponse to ecdysone ;direct assaynegative regulation of transcription, DNA-templated; segment specification ;
FBgn0036660 -	interstrand cross-link repair ;protein ubiquitination
FBgn0037975 -	oxidation-reduction process ;
FBgn0039419	pathway ;norepinephrine-epinephrine vasoconstriction involved in regulation of systemic arterial blood pressure
Thioester-containing protein 2	defense response to Gram-negative bacterium; innate immune response ;genetic interaction with Tep4, Tep3, Tep1
golden goal	axon guidance; photoreceptor cell axon guidance; retinal ganglion cell axon guidance ;
Chronologically inappropriate morphogenesis	regulation of actin filament polymerization; neuron development; male somatic sex determination; regulation of stem cell division; eye-antennal disc development; negative regulation of protein phosphorylation; mushroom body development ;
aurora borealis	regulation of mitotic nuclear division ;regulation of mitotic spindle organization ;activation of protein kinase activity ;asymmetric protein localization involved in cell fate determination; activation of protein kinase activity ;
Protein tyrosine phosphatase 61F	peptidyl-tyrosine dephosphorylation; negative regulation of ERK1 and ERK2 cascade; negative regulation of insulin receptor signaling pathway ;negative regulation of phosphatidylinositol 3-kinase signaling ; axon guidance ;genetic interaction with Ras85D
corolla	in reciprocal meiotic recombination; centromere clustering; female meiotic nuclear division

Supplementary Table 5. Overrepresented GO terms associated with differentially expressed genes from batch 1. Terms listed are significantly enriched as determined by a Fisher's Exact test and FDR threshold of 0.10. Terms related to meiotic or mitotic cell division are highlighted in bold. Terms are listed in order of descending enrichment score.

GO biological process	number genes in genome	number DE genes	enrichment	FDR
spindle midzone assembly	5	5	12.89	0.00754
cytoplasmic translation	119	79	8.56	1.49E-35
mitotic spindle elongation	8	5	8.06	0.0274
kinetochore organization	8	5	8.06	0.0273
attachment of spindle microtubules to kinetochore	10	6	7.73	0.0121
mitotic spindle assembly checkpoint	14	8	7.37	0.00237
negative regulation of phosphatidylinositol 3-kinase signaling	9	5	7.16	0.0372
centrosome separation	19	10	6.78	0.000634
regulation of sevenless signaling pathway	10	5	6.45	0.0486
regulation of compound eye photoreceptor development	12	6	6.45	0.0223
ribosomal large subunit assembly	20	10	6.45	0.000866
DNA unwinding involved in DNA replication	10	5	6.45	0.0485
positive regulation of compound eye photoreceptor cell differentiation	10	5	6.45	0.0484
mitotic spindle assembly checkpoint	14	8	7.37	0.00237
mitotic spindle assembly	25	12	6.19	0.000217
axon extension	35	15	5.52	5.28E-05
ribosomal small subunit assembly	25	10	5.16	0.00305
nuclear DNA replication	18	7	5.01	0.0272
female meiosis chromosome segregation	34	13	4.93	0.000571
metaphase plate congression	21	8	4.91	0.0151
maturat ion of LSU-rRNA	21	8	4.91	0.0151
establishment or maintenance of polarity of follicular epithelium	29	11	4.89	0.00226
ecdysteroid biosynthetic process	19	7	4.75	0.033
mitotic cell cycle, embryonic	30	11	4.73	0.00273
snRNA 3'-end processing	22	8	4.69	0.0186
cell cycle comprising mitosis without cytokinesis	20	7	4.51	0.0403
regulation of nucleocytoplasmic transport	26	9	4.46	0.013
ATP synthesis coupled proton transport	24	8	4.3	0.028
microtubule polymerization or depolymerization	30	10	4.3	0.00873
microtubule polymerization	24	8	4.3	0.0279
regulation of hippo signaling	37	12	4.18	0.00329
nuclear migration	32	10	4.03	0.0128
negative regulation of cellular response to growth factor stimulus	29	9	4	0.0225
negative regulation of cytoskeleton organization	33	10	3.91	0.0152
regulation of organelle assembly	30	9	3.87	0.027
DNA biosynthetic process	40	12	3.87	0.00565
regulation of cell division	44	13	3.81	0.00377
maturat ion of SSU-rRNA from tricistronic rRNA transcript (SSU-rRNA, 5.8S rRNA, LSU-rRNA)	33	9	3.52	0.0417
cytokinetic process	38	10	3.39	0.0327
protein autophosphorylation	39	10	3.31	0.0374
dorsal/ventral axis specification	72	18	3.22	0.00173
negative regulation of neurogenesis	77	19	3.18	0.00132
regulation of microtubule cytoskeleton organization	57	14	3.17	0.00964
meiotic cytokinesis	45	11	3.15	0.0327
cortical actin cytoskeleton organization	51	12	3.03	0.028
male meiotic nuclear division	81	19	3.02	0.00219
imaginal disc-derived wing hair organization	47	11	3.02	0.0413
wing disc pattern formation	80	18	2.9	0.00445
negative regulation of cell population proliferation	86	19	2.85	0.00377

GO biological process	number genes in genome	number DE genes	enrichment	FDR
imaginal disc-derived wing vein specification	55	12	2.81	0.0437
positive regulation of apoptotic process	69	15	2.8	0.0171
protein-DNA complex assembly	74	16	2.79	0.0128
actomyosin structure organization	84	18	2.76	0.00704
chromatin remodeling	103	22	2.75	0.00212
striated muscle cell development	61	13	2.75	0.0373
programmed cell death involved in cell development	86	18	2.7	0.00874
regulation of chromatin organization	111	23	2.67	0.00303
negative regulation of phosphorylation	68	14	2.65	0.0343
positive regulation of compound eye photoreceptor cell differentiation	10	5	6.45	0.0484
regulation of compound eye photoreceptor cell differentiation	34	11	4.17	0.00586
compound eye photoreceptor cell differentiation	153	31	2.61	0.000279
regulation of protein kinase activity	90	18	2.58	0.0184
regulation of autophagy	106	21	2.55	0.00744
regulation of supramolecular fiber organization	96	19	2.55	0.0142
eggshell chorion assembly	87	17	2.52	0.0281
regulation of Ras protein signal transduction	87	17	2.52	0.028
asymmetric cell division	103	20	2.5	0.0119
regulation of gene silencing	89	17	2.46	0.0313
oxidative phosphorylation	92	17	2.38	0.0376
negative regulation of protein modification process	93	17	2.36	0.0403
dorsal closure	106	19	2.31	0.0401
establishment of planar polarity	96	17	2.28	0.0487
positive regulation of organelle organization	144	25	2.24	0.0103
transcription, DNA-templated	185	31	2.16	0.00571
negative regulation of transcription, DNA-templated	365	53	1.87	0.00138
regulation of transcription, DNA-templated	1121	154	1.77	5.93E-09
positive regulation of transcription, DNA-templated	450	61	1.75	0.00219
positive regulation of protein modification process	159	26	2.11	0.0171
histone modification	181	29	2.07	0.0132
negative regulation of transcription by RNA polymerase II	216	33	1.97	0.014
positive regulation of catalytic activity	177	27	1.97	0.0384
regulation of cellular component size	180	27	1.93	0.0416
protein ubiquitination	182	27	1.91	0.0441
axon guidance	263	39	1.91	0.00867
embryonic pattern specification	199	29	1.88	0.0431
central nervous system development	268	39	1.88	0.0101
positive regulation of signal transduction	365	53	1.87	0.00138
cellular response to DNA damage stimulus	215	31	1.86	0.0411
regulation of cell fate commitment	40	10	3.22	0.0422
cell fate commitment	294	41	1.8	0.016
regulation of growth	304	42	1.78	0.0186
positive regulation of transcription, DNA-templated	450	61	1.75	0.00219
regulation of intracellular signal transduction	331	53	2.06	0.000168
intracellular signal transduction	376	49	1.68	0.0208
protein localization	699	78	1.44	0.043
response to bacterium	246	7	0.37	0.0485
sensory perception of chemical stimulus	273	6	0.28	0.00566
detection of chemical stimulus	166	3	0.23	0.0412
chitin metabolic process	117	0	< 0.01	0.00537

Supplementary Table 6. Overrepresented GO terms associated with differentially expressed genes from batch 2. No terms were significant after FDR correction, so the terms with a raw p-value < 0.05 are listed. Terms related to meiotic or mitotic cell division are highlighted in bold. Terms are listed in order of descending enrichment score.

GO biological process	number genes in genome	number DE genes	enrichment	raw p-value
N-acetylineuraminate catabolic process	1	1	> 100	0.0127
regulation of histone H4 acetylation involved in response to DNA damage stimulus	1	1	> 100	0.0127
maintenance of rDNA	1	1	> 100	0.0127
glucosamine catabolic process	1	1	> 100	0.0127
positive regulation of compound eye retinal cell apoptotic process	1	1	> 100	0.0127
negative regulation of synaptic vesicle fusion to presynaptic active zone membrane	1	1	> 100	0.0127
regulation of plasma membrane organization	1	1	> 100	0.0127
centromere clustering	1	1	> 100	0.0127
negative regulation of vascular endothelial growth factor receptor signaling pathway	2	1	78.22	0.0189
male somatic sex determination	2	1	78.22	0.0189
female meiosis sister chromatid cohesion	2	1	78.22	0.0189
cysteinyl-tRNA aminoacylation	2	1	78.22	0.0189
regulation of gene expression by genetic imprinting	2	1	78.22	0.0189
internal genitalia morphogenesis	2	1	78.22	0.0189
DNA damage response, signal transduction by p53				
class mediator	2	1	78.22	0.0189
permeability involved in programmed necrotic cell death	2	1	78.22	0.0189
meiotic DNA double-strand break processing				
involved in reciprocal meiotic recombination	2	1	78.22	0.0189
negative regulation of insulin secretion	2	1	78.22	0.0189
positive regulation of DNA topoisomerase (ATP-hydrolyzing) activity	2	1	78.22	0.0189
N-acetylglucosamine catabolic process	2	1	78.22	0.0189
establishment of sister chromatid cohesion	3	1	52.15	0.0252
cilium movement involved in cell motility	6	2	52.15	0.00109
gamma-aminobutyric acid signaling pathway	3	1	52.15	0.0252
cytolysis	3	1	52.15	0.0252
positive regulation of transcription by RNA polymerase III	3	1	52.15	0.0252
regulation of chromatin binding	4	1	39.11	0.0314
morphogenesis	4	1	39.11	0.0314
regulation of cytokinesis, actomyosin contractile ring assembly	4	1	39.11	0.0314
UDP-N-acetylglucosamine biosynthetic process	4	1	39.11	0.0314
positive regulation of ribosome biogenesis	4	1	39.11	0.0314
regulation of mitotic spindle organization	5	1	31.29	0.0375
male meiosis sister chromatid cohesion	5	1	31.29	0.0375
positive regulation of RNA export from nucleus	5	1	31.29	0.0375
maintenance of protein location in nucleus	5	1	31.29	0.0375
inner dynein arm assembly	6	1	26.07	0.0436
synaptonemal complex assembly	6	1	26.07	0.0436
poly(A)+ mRNA export from nucleus	12	2	26.07	0.00345
activity	6	1	26.07	0.0436
vitelline membrane formation involved in chorion-containing eggshell formation	13	2	24.07	0.00397
dosage compensation by hyperactivation of X chromosome	13	2	24.07	0.00397
primary miRNA processing	7	1	22.35	0.0497
negative regulation of hemocyte proliferation	7	1	22.35	0.0497
cellular response to mechanical stimulus	7	1	22.35	0.0497

GO biological process	number genes in genome	number DE genes	enrichment	raw p-value
DNA topological change	7	1	22.35	0.0497
histone H4-K16 acetylation	7	1	22.35	0.0497
positive regulation of transcription of nucleolar large rRNA by RNA polymerase I	7	1	22.35	0.0497
axis elongation	7	1	22.35	0.0497
male sex differentiation	30	2	10.43	0.0175
positive regulation of actin filament polymerization	31	2	10.09	0.0185
activation of protein kinase activity	33	2	9.48	0.0207
flagellated sperm motility	34	2	9.2	0.0218
regulation of G2/M transition of mitotic cell cycle	34	2	9.2	0.0218
DNA integrity checkpoint	38	2	8.23	0.0266
glutathione metabolic process	50	2	6.26	0.0431
central nervous system development	268	5	2.92	0.0299

REFERENCES CITED

- Adrian, A. B., & Comeron, J. M. (2013). The *Drosophila* early ovarian transcriptome provides insight to the molecular causes of recombination rate variation across genomes. *BMC Genomics*, 14, 794. <https://doi.org/10.1186/1471-2164-14-794>
- Aguilera, A., & Gaillard, H. (2014). Transcription and recombination: when RNA meets DNA. *Cold Spring Harbor Perspectives in Biology*, 6(8), a016543. <https://doi.org/10.1101/cshperspect.a016543>
- Andronic, L. (2012). Viruses as triggers of DNA rearrangements in host plants. *Canadian Journal of Plant Science*, 92(6), 1083–1091. <https://doi.org/10.1139/CJPS2011-197>
- Aprianto, R., Slager, J., Holsappel, S., & Veening, J.-W. (2018). High-resolution analysis of the pneumococcal transcriptome under a wide range of infection-relevant conditions. *Nucleic Acids Research*, 46(19), 9990–10006. <https://doi.org/10.1093/nar/gky750>
- Ballard, J. W. O. (2004). Sequential Evolution of a Symbiont Inferred From the Host: Wolbachia and *Drosophila simulans*. *Molecular Biology and Evolution*, 21(3), 428–442. <https://doi.org/10.1093/molbev/msh028>
- Balyaev DK and Borodin PM. (1982). The influence of stress on variation and its role in evolution. *Biol. Zentbl.*, 100, 705–714.
- Beckmann, J. F., Ronau, J. A., & Hochstrasser, M. (2017). A Wolbachia deubiquitylating enzyme induces cytoplasmic incompatibility. *Nature Microbiology*, 2, 17007. <https://doi.org/10.1038/nmicrobiol.2017.7>
- Bing, X., Attardo, G. M., Vigneron, A., Aksoy, E., Scolari, F., Malacrida, A., Weiss, B. L., & Aksoy, S. (2017). Unravelling the relationship between the tsetse fly and its obligate symbiont *Wigglesworthia*: transcriptomic and metabolomic landscapes reveal highly integrated physiological networks. *Proceedings. Biological Sciences*, 284(1857), 20170360. <https://doi.org/10.1098/rspb.2017.0360>
- Bourtzis, K., Nirgianaki, A., Markakis, G., & Savakis, C. (1996). Wolbachia Infection and Cytoplasmic Incompatibility in *Drosophila* Species. *Genetics*, 144(3), 1063. <http://www.genetics.org/content/144/3/1063.abstract>
- Bradshaw, A. D. (1965). Evolutionary Significance of Phenotypic Plasticity in Plants. *Advances in Genetics*, 13, 115–155. [https://doi.org/10.1016/S0065-2660\(08\)60048-6](https://doi.org/10.1016/S0065-2660(08)60048-6)
- Brakefield, P. M. (2008). Tropical dry and wet season polyphenism in the butterfly *Melanitis leda* (Satyrinae): Phenotypic plasticity and climatic correlates. *Biological Journal of the Linnean Society*, 31(2), 175–191. <https://doi.org/10.1111/j.1095-8312.1987.tb01988.x>

- Brehm, V. (1909). Über die Nackenzähne der Daphnien. *International Revue Der Gesamten Hydrobiologie Und Hydrographie*, 2(4-5), 749-753.
doi.org/10.1002/iroh.19090020410.
- Brem, R. B., Yvert, G., Clinton, R., & Kruglyak, L. (2002). Genetic Dissection of Transcriptional Regulation in Budding Yeast. *Science*, 296(5568), 752.
<https://doi.org/10.1126/science.1069516>
- Brennan, L. J., Keddie, B. A., Braig, H. R., & Harris, H. L. (2008). The endosymbiont Wolbachia pipiens induces the expression of host antioxidant proteins in an Aedes albopictus cell line. *PloS One*, 3(5), e2083. doi.org/10.1371/journal.pone.0002083
- Brownlie, J. C., Cass, B. N., Riegler, M., Witsenburg, J. J., Iturbe-Ormaetxe, I., McGraw, E. A., & O'Neill, S. L. (2009). Evidence for Metabolic Provisioning by a Common Invertebrate Endosymbiont, Wolbachia pipiens, during Periods of Nutritional Stress. *PLOS Pathogens*, 5(4) e1000368. doi.org/10.1371/journal.ppat.1000368
- Camillos-Neto, D., Bonato, P., Wassem, R., Tadra-Sfeir, M. Z., Brusamarello-Santos, L. C. C., Valdameri, G., Donatti, L., Faoro, H., Weiss, V. A., Chubatsu, L. S., Pedrosa, F. O., & Souza, E. M. (2014). Dual RNA-seq transcriptional analysis of wheat roots colonized by Azospirillum brasilense reveals up-regulation of nutrient acquisition and cell cycle genes. *BMC Genomics*, 15(1), 378. <https://doi.org/10.1186/1471-2164-15-378>
- Chevalier, F., Herbinière-Gaboreau, J., Charif, D., Mitta, G., Gavory, F., Wincker, P., Grève, P., Braquart-Varnier, C., & Bouchon, D. (2012). Feminizing Wolbachia: a transcriptomics approach with insights on the immune response genes in *Armadillidium vulgare*. *BMC Microbiology* doi.org/10.1186/1471-2180-12-S1-S1
- Dixon, A. L., Liang, L., Moffatt, M. F., Chen, W., Heath, S., Wong, K. C. C., Taylor, J., Burnett, E., Gut, I., Farrall, M., Lathrop, G. M., Abecasis, G. R., & Cookson, W. O. C. (2007). A genome-wide association study of global gene expression. *Nature Genetics*, 39(10), 1202–1207. <https://doi.org/10.1038/ng2109>
- Fast, E. M., Toomey, M. E., Panaram, K., Desjardins, D., Kolaczyk, E. D., & Frydman, H. M. (2011). Wolbachia Enhance Drosophila Stem Cell Proliferation and Target the Germline Stem Cell Niche. *Science*, 334(6058), 990.
doi.org/10.1126/science.1209609
- Fry, A J, Palmer, M. R., & Rand, D. M. (2004). Variable fitness effects of Wolbachia infection in *Drosophila melanogaster*. *Heredity*, 93(4), 379-389.
doi.org/10.1038/sj.hdy.6800514
- Fry, Adam J, & Rand, D. M. (2002). WOLBACHIA INTERACTIONS THAT DETERMINE DROSOPHILA MELANOGASTER SURVIVAL. *Evolution*, 56(10), 1976–1981. <https://doi.org/10.1111/j.0014-3820.2002.tb00123.x>

- Gao, J., Davidson, M. K., & Wahls, W. P. (2008). Distinct regions of ATF/CREB proteins Atf1 and Pcr1 control recombination hotspot ade6-M26 and the osmotic stress response. *Nucleic Acids Research*, 36(9), 2838–2851. <https://doi.org/10.1093/nar/gkn037>
- Gottipati, P., & Helleday, T. (2009). Transcription-associated recombination in eukaryotes: link between transcription, replication and recombination. *Mutagenesis*, 24(3), 203–210. <https://doi.org/10.1093/mutage/gen072>
- Grobler, Y., Yun, C. Y., Kahler, D. J., Bergman, C. M., Lee, H., Oliver, B., & Lehmann, R. (2018). Whole genome screen reveals a novel relationship between Wolbachia levels and Drosophila host translation. *PLoS Pathogens*, 14(11), e1007445–e1007445. <https://doi.org/10.1371/journal.ppat.1007445>
- Gruntenko, N. E., Ilinsky, Y. Yu., Adonyeva, N. v., Burdina, E. v., Bykov, R. A., Menshanov, P. N., & Rauschenbach, I. Yu. (2017). Various Wolbachia genotypes differently influence host Drosophila dopamine metabolism and survival under heat stress conditions. *BMC Evolutionary Biology*, 17(2), 252. <https://doi.org/10.1186/s12862-017-1104-y>
- Hilgenboecker, K., Hammerstein, P., Schlattmann, P., Telschow, A., & Werren, J. H. (2008). How many species are infected with Wolbachia?--A statistical analysis of current data. *FEMS Microbiology Letters*, 281(2), 215–220. <https://doi.org/10.1111/j.1574-6968.2008.01110.x>
- Hosokawa, T., Koga, R., Kikuchi, Y., Meng, X.-Y., & Fukatsu, T. (2010). Wolbachia as a bacteriocyte-associated nutritional mutualist. *Proceedings of the National Academy of Sciences*, 107(2), 769. <https://doi.org/10.1073/pnas.0911476107>
- Huang, W., Carbone, M. A., Magwire, M. M., Peiffer, J. A., Lyman, R. F., Stone, E. A., Anholt, R. R. H., & Mackay, T. F. C. (2015). Genetic basis of transcriptome diversity in *Drosophila melanogaster*; *Proceedings of the National Academy of Sciences*, 112(44), E6010. <https://doi.org/10.1073/pnas.1519159112>
- Hughes, G. L., Ren, X., Ramirez, J. L., Sakamoto, J. M., Bailey, J. A., Jedlicka, A. E., & Rasgon, J. L. (2011). Wolbachia infections in *Anopheles gambiae* cells: transcriptomic characterization of a novel host-symbiont interaction. *PLoS Pathogens*, 7(2), e1001296–e1001296. <https://doi.org/10.1371/journal.ppat.1001296>
- Hunter, C. M., Huang, W., Mackay, T. F. C., & Singh, N. D. (2016). The Genetic Architecture of Natural Variation in Recombination Rate in *Drosophila melanogaster*. *PLOS Genetics*, 12(4), e1005951-doi.org/10.1371/journal.pgen.1005951

- Hussin, J., Roy-Gagnon, M.-H., Gendron, R., Andelfinger, G., & Awadalla, P. (2011). Age-Dependent Recombination Rates in Human Pedigrees. *PLOS Genetics*, 7(9), e1002251-. <https://doi.org/10.1371/journal.pgen.1002251>
- Hutter, S., Saminadin-Peter, S. S., Stephan, W., & Parsch, J. (2008). Gene expression variation in African and European populations of *Drosophila melanogaster*. *Genome Biology*, 9(1), R12–R12. <https://doi.org/10.1186/gb-2008-9-1-r12>
- Ko, D. C., Shukla, K. P., Fong, C., Wasnick, M., Brittnacher, M. J., Wurfel, M. M., Holden, T. D., O'Keefe, G. E., van Yserloo, B., Akey, J. M., & Miller, S. I. (2009). A genome-wide in vitro bacterial-infection screen reveals human variation in the host response associated with inflammatory disease. *American Journal of Human Genetics*, 85(2), 214–227. <https://doi.org/10.1016/j.ajhg.2009.07.012>
- Kon, N., Schroeder, S. C., Krawchuk, M. D., & Wahls, W. P. (1998). Regulation of the Mts1-Mts2-dependent ade6-M26 meiotic recombination hot spot and developmental decisions by the Spc1 mitogen-activated protein kinase of fission yeast. *Molecular and Cellular Biology*, 18(12), 7575–7583. <https://doi.org/10.1128/mcb.18.12.7575>
- Kremer, N., Charif, D., Henri, H., Gavory, F., Wincker, P., Mavingui, P., & Vavre, F. (2012). Influence of Wolbachia on host gene expression in an obligatory symbiosis. *BMC Microbiology*, 12 Suppl 1(Suppl 1), S7–S7. <https://doi.org/10.1186/1471-2180-12-S1-S7>
- Kriesner, P., Hoffmann, A. A., Lee, S. F., Turelli, M., & Weeks, A. R. (2013). Rapid Sequential Spread of Two Wolbachia Variants in *Drosophila simulans*. *PLOS Pathogens*, 9(9), e1003607-. <https://doi.org/10.1371/journal.ppat.1003607>
- LePage, D. P., Metcalf, J. A., Bordenstein, S. R., On, J., Perlmuter, J. I., Shropshire, J. D., Layton, E. M., Funkhouser-Jones, L. J., Beckmann, J. F., & Bordenstein, S. R. (2017). Prophage WO genes recapitulate and enhance Wolbachia-induced cytoplasmic incompatibility. *Nature*, 543(7644), 243–247. <https://doi.org/10.1038/nature21391>
- Manheim, E. A., & McKim, K. S. (2003). The Synaptonemal Complex Component C(2)M Regulates Meiotic Crossing over in *Drosophila*. *Current Biology*, 13(4), 276–285. [https://doi.org/10.1016/S0960-9822\(03\)00050-2](https://doi.org/10.1016/S0960-9822(03)00050-2)
- Maslowski, K. M. (2019). Metabolism at the centre of the host–microbe relationship. *Clinical & Experimental Immunology*, 197(2), 193–204. <https://doi.org/10.1111/cei.13329>
- Mateus, I. D., Masclaux, F. G., Aletti, C., Rojas, E. C., Savary, R., Dupuis, C., & Sanders, I. R. (2019). Dual RNA-seq reveals large-scale non-conserved genotype × genotype-specific genetic reprogramming and molecular crosstalk in the

mycorrhizal symbiosis. *The ISME Journal*, 13(5), 1226–1238. <https://doi.org/10.1038/s41396-018-0342-3>

McKim, K. S., Jang, J. K., & Manheim, E. A. (2002). Meiotic Recombination and Chromosome Segregation in Drosophila Females. *Annual Review of Genetics*, 36(1), 205–232. <https://doi.org/10.1146/annurev.genet.36.041102.113929>

Miller, W., Ehrman, L., Schneider, D. (2010). Infectious Speciation Revisited: Impact of Symbiont-Depletion on Female Fitness and Mating Behavior of *Drosophila paulistorum*. *PLOS Pathogens*, 6(12), e1001214. doi.org/10.1371/journal.ppat.1001214

Modliszewski, J. L., & Copenhaver, G. P. (2017). Meiotic recombination gets stressed out: CO frequency is plastic under pressure. *Current Opinion in Plant Biology*, 36, 95–102. <https://doi.org/10.1016/J.PBI.2016.11.019>

Molloy, J. C., Sommer, U., Viant, M. R., & Sinkins, S. P. (2016). Wolbachia Modulates Lipid Metabolism in *Aedes albopictus* Mosquito Cells. *Applied and Environmental Microbiology*, 82(10), 3109. <https://doi.org/10.1128/AEM.00275-16>

Neel, J. v. (1941). A RELATION BETWEEN LARVAL NUTRITION AND THE FREQUENCY OF CROSSING OVER IN THE THIRD CHROMOSOME OF DROSOPHILA MELANOGASTER. *Genetics*, 26(5), 506. <http://www.genetics.org/content/26/5/506.abstract>

Nuss, A. M., Beckstette, M., Pimenova, M., Schmühl, C., Opitz, W., Pisano, F., Heroven, A. K., & Dersch, P. (2017). Tissue dual RNA-seq allows fast discovery of infection-specific functions and riboregulators shaping host-pathogen transcriptomes. *Proceedings of the National Academy of Sciences*, 114(5), E791. <https://doi.org/10.1073/pnas.1613405114>

Pan, X., Zhou, G., Wu, J., Bian, G., Lu, P., Raikhel, A. S., & Xi, Z. (2012). Wolbachia induces reactive oxygen species (ROS)-dependent activation of the Toll pathway to control dengue virus in the mosquito *Aedes aegypti*. *Proceedings of the National Academy of Sciences of the United States of America*, 109(1), E23–E31. <https://doi.org/10.1073/pnas.1116932108>

Plough, H. H. (1917). The effect of temperature on crossingover in *Drosophila*. *Journal of Experimental Zoology*, 24(2), 147–209. <https://doi.org/10.1002/jez.1400240202>

Poelstra, J., Vijay, N., Bossu, C., Lantz, H., Ryall, B., Müller, I., Baglione, V., Unneberg, P., Wikelski, M., Grabherr, M., & Wolf, J. (2014). The genomic landscape underlying phenotypic integrity in the face of gene flow in crows. *Science (New York, N.Y.)*, 344, 1410–1414. <https://doi.org/10.1126/science.1253226>

- Rao, R. U., Huang, Y., Abubucker, S., Heinz, M., Crosby, S. D., Mitreva, M., & Weil, G. J. (2012). Effects of doxycycline on gene expression in Wolbachia and *Brugia malayi* adult female worms *in vivo*. *Journal of Biomedical Science*, 19(1), 21. <https://doi.org/10.1186/1423-0127-19-21>
- Reynolds, A., Qiao, H., Yang, Y., Chen, J. K., Jackson, N., Biswas, K., Holloway, J. K., Baudat, F., de Massy, B., Wang, J., Höög, C., Cohen, P. E., & Hunter, N. (2013). RNF212 is a dosage-sensitive regulator of crossing-over during mammalian meiosis. *Nature Genetics*, 45(3), 269–278. <https://doi.org/10.1038/ng.2541>
- Rienksma, R. A., Schaap, P. J., Martins Dos Santos, V. A. P., & Suarez-Diez, M. (2019). Modeling Host-Pathogen Interaction to Elucidate the Metabolic Drug Response of Intracellular *Mycobacterium tuberculosis*. *Frontiers in Cellular and Infection Microbiology*, 9, 144. <https://doi.org/10.3389/fcimb.2019.00144>
- Scheepens, J. F., Deng, Y., & Bossdorf, O. (2018). Phenotypic plasticity in response to temperature fluctuations is genetically variable, and relates to climatic variability of origin, in *Arabidopsis thaliana*. *AoB PLANTS*, 10(4), ply043–ply043. <https://doi.org/10.1093/aobpla/ply043>
- Serga, S., Maistrenko, O., Rozhok, A., Mousseau, T., & Kozeretska, I. (2014). Fecundity as one of possible factors contributing to the dominance of the wMel genotype of Wolbachia in natural populations of *Drosophila melanogaster*. *Symbiosis*, 63(1), 11–17. <https://doi.org/10.1007/s13199-014-0283-1>
- Singh, N. D. (2019). Wolbachia Infection Associated with Increased Recombination in *Drosophila*. *G3: Genes|Genomes|Genetics*, 9(1), 229. doi.org/10.1534/g3.118.200827
- Small, C. M., Milligan-Myhre, K., Bassham, S., Guillemin, K., & Cresko, W. A. (2017). Host Genotype and Microbiota Contribute Asymmetrically to Transcriptional Variation in the Threespine Stickleback Gut. *Genome Biology and Evolution*, 9(3), 504–520. <https://doi.org/10.1093/gbe/evx014>
- Solignac, M., Vautrin, D., & Rousset, F. (1994). Widespread occurrence of the proteobacteria Wolbachia and partial cytoplasmic incompatibility in *Drosophila melanogaster*. *Comptes Rendus de l'Academie Des Sciences - Serie III*, 317, 461–470.
- Stapley, J., Feulner, P. G. D., Johnston, S. E., Santure, A. W., & Smadja, C. M. (2017). Variation in recombination frequency and distribution across eukaryotes: patterns and processes. *Philosophical Transactions of the Royal Society B: Biological Sciences*, 372(1736), 20160455. <https://doi.org/10.1098/rstb.2016.0455>

- Stern, C. (1926). An Effect of Temperature and Age on Crossing-Over in the First Chromosome of *Drosophila Melanogaster*. *Proceedings of the National Academy of Sciences*, 12(8), 530. <https://doi.org/10.1073/pnas.12.8.530>
- Tollrian, R. (1995). Predator-Induced Morphological Defenses: Costs, Life History Shifts, and Maternal Effects in *Daphnia Pulex*. *Ecology*, 76(6), 1691–1705. <https://doi.org/10.2307/1940703>
- Vavre, F., Girin, C., & Boulétreau, M. (1999). Phylogenetic status of a fecundity-enhancing Wolbachia that does not induce thelytoky in *Trichogramma*. *Insect Molecular Biology*, 8(1), 67–72. <https://doi.org/10.1046/j.1365-2583.1999.810067.x>
- Verbon, E. H., & Liberman, L. M. (2016). Beneficial Microbes Affect Endogenous Mechanisms Controlling Root Development. *Trends in Plant Science*, 21(3), 218–229. <https://doi.org/10.1016/j.tplants.2016.01.013>
- Weeks, A. R., Turelli, M., Harcombe, W. R., Reynolds, K. T., & Hoffmann, A. A. (2007). From Parasite to Mutualist: Rapid Evolution of Wolbachia in Natural Populations of *Drosophila*. *PLOS Biology*, 5(5), e114. <https://doi.org/10.1371/journal.pbio.0050114>
- Werren, J. H., Baldo, L., & Clark, M. E. (2008). Wolbachia: master manipulators of invertebrate biology. *Nature Reviews Microbiology*, 6(10), 741–751. <https://doi.org/10.1038/nrmicro1969>
- Xi, Z., Gavotte, L., Xie, Y., & Dobson, S. L. (2008). Genome-wide analysis of the interaction between the endosymbiotic bacterium Wolbachia and its *Drosophila* host. *BMC Genomics*, 9, 1. <https://doi.org/10.1186/1471-2164-9-1>
- Zheng, Y., Wang, J.-L., Liu, C., Wang, C.-P., Walker, T., & Wang, Y.-F. (2011). Differentially expressed profiles in the larval testes of Wolbachia infected and uninfected *Drosophila*. *BMC Genomics*, 12, 595. <https://doi.org/10.1186/1471-2164-12-595>
- Zilio, G., Moesch, L., Bovet, N., Sarr, A., & Koella, J. C. (2018). The effect of parasite infection on the recombination rate of the mosquito *Aedes aegypti*. *PLOS ONE*, 13(10), e0203481-. <https://doi.org/10.1371/journal.pone.0203481>
- Ziolkowski, P. A., Underwood, C. J., Lambing, C., Martinez-Garcia, M., Lawrence, E. J., Ziolkowska, L., Griffin, C., Choi, K., Franklin, F. C. H., Martienssen, R. A., & Henderson, I. R. (2017). Natural variation and dosage of the HEI10 meiotic E3 ligase control *Arabidopsis* crossover recombination. *Genes & Development*, 31(3), 306–317. <https://doi.org/10.1101/gad.295501.116>

Zug, R., & Hammerstein, P. (2012). Still a Host of Hosts for Wolbachia: Analysis of Recent Data Suggests That 40% of Terrestrial Arthropod Species Are Infected. *PLOS ONE*, 7(6), e38544-. <https://doi.org/10.1371/journal.pone.0038544>